The effects of climate change on water resources in central Sweden simulated by the two conceptual models HBV and WASMOD

GEO4320 - Hydrological Modeling, UiO
Jouval Somer
Fall 2023

Abstract

This study employs the Hydrologiska Byråns Vattenbalansavdelning (HBV) and Water and Snow Balance Modeling System (WASMOD) models to analyze the impact of climate change on water resources in the Åkesta catchment, central Sweden. Utilizing observed data, the models are calibrated and applied to three climate change scenarios: Scenario 1 ($\Delta T = +3C$, $\Delta P = 0\%$), Scenario 2 ($\Delta T = +3C$, $\Delta P = +15\%$), and Scenario 3 ($\Delta T = +3C$, $\Delta P = -15\%$). Key findings include a consistent leftward shift in peak discharge across scenarios, indicative of earlier peak flows, and a general reduction in peak discharge magnitudes, highlighting potential water availability challenges. The WASMOD model shows increased evapotranspiration peaks, while both models predict a significant reduction in snowpack peaks, particularly under decreased precipitation. These results underline the complexity of hydrological responses to climate change and the importance of using multiple models for robust analysis and informed water resource management in changing climates.

1 Introduction

Climate change remains one of the most compelling global challenges we have faced and is an ever-growing concern for humanity and our planet. It has far-reaching consequences that extend into various sectors, including water resources. Therefore, it is crucial for us to better understand the hydrological implications these changes have on our society and water resources. A trivial way to do so is by employing hydrological models which offer an invaluable understanding of the complex relationship between climate and water resources.

In this study we will utilise two different hydrological models, the Hydrologiska Byråns Vattenbalansavdelning (HBV) model and the water and snow balance modeling system (WASMOD). These models are both conceptual and lumped based models.

The models will first be calibrated (optimized) and verified manually. For the HBV this is done using physical intuition for how the different parameters affect the model outcome. Whilst, for the WASMOD the prosses is more automized, and the manual aspects primarily include model selection.

Then, the split-sample verification method [Arsenault et al., 2018] is employed in order to establish a better understanding of how the models perform in unseen circumstances. Parameter sensitivity and uncertainty analysis is then done on the two methods by setting physically plausible ranges for the model parameters, and a Monte Carlo optimization simulation is run to randomly navigate the complex parameter space [Khu and Werner, 2003]. After model limitations and ranges for robustness are established, the models are employed on three different climate change scenarios by modifying the historical time series used as model input. The three scenarios include:

- Scenario 1: $\Delta T = +3C$, $\Delta P = 0\%$,
- Scenario 2: $\Delta T = +3C$, $\Delta P = +15\%$,
- Scenario 3: $\Delta T = +3C$, $\Delta P = -15\%$.

Where ΔT is the change in temterature and ΔP is the change in precipitation.

2 Study Area and Data

The chosen catchment for this study is Åkesta at Kvarn, situated in central Sweden, encompassing an area of $730 km^2$. The data, spanning from 1981

to 1991, comprises 11 years of daily observed precipitation, temperature, and discharge, making it an ideal dataset for our evaluation.

3 Models and Methodology

In this section, the different model performance measures used to assess and calibrate the models used in this study are explored. Additionally, we will describe how the models were calibrated and validated, and lastly present the optimum models.

3.1 Model Performance Measures

3.1.1 Model Efficiency, R_{eff}

Model Efficiency, often denoted as "R_{eff}" or "E," quantifies the ability of a hydrological model to replicate observed data, typically streamflow or runoff. It is a dimensionless statistic that assesses the relative quality of model simulations compared to the observed values. The R_{eff} value is calculated as follows:

$$R_{\text{eff}} = 1 - \frac{\sum \left(Q_{\text{sim}}(t) - Q_{\text{obs}}(t)\right)^2}{\sum \left(Q_{\text{obs}}(t) - \bar{Q}_{\text{obs}}\right)^2}. \qquad (1)$$

The R_{eff} compares the prediction by the model with the simplest possible prediction, a constant value of the observed mean value over the entire period. [Seibert, 1996]

$R_{\text{eff}} = 1$ Perfect fit, $Q_{\text{Sim}}(t) = Q_{\text{obs}}(t)$,

$R_{\text{eff}} = 0$ Simulation as good (or poor) as the constant-value ,

$R_{\text{eff}} < 0$ Very poor fit,

Note, the terms Nash-Sutcliffe coefficient, Model Efficiency, Reff, R_{eff} and R2, will be used somewhat interchangeably in this study. Regardless, Equation 1 is what is meant.

3.1.2 Mean Difference

The Mean Difference, often denoted as MeanDiff, is a statistical metric used to quantify the average discrepancy between the model's simulated values and the observed data. It is calculated as follows:

$$\text{MeanDiff} = \frac{\sum \left(Q_{obs} - Q_{\text{sim}}\right)}{\text{No of days}} 365, \qquad (2)$$

and has units of [mm/year].

The Mean Difference value provides insight into how closely the model's simulations match the observed data. A lower Mean Difference indicates that the model's results are closer to the observed values, suggesting better model performance. Conversely, a higher Mean Difference suggests that the model's simulations deviate more from the observed data, indicating potential shortcomings in the model. The value for "perfect" fit for the Mean difference is 0 [mm/year][Seibert, 1996].

3.1.3 Visual Measures

Lastly, we will use visual measures to assess the models' performance. These include plotting the simulated and observed discharges, Q_{sim} and Q_{obs} respectively, and comparing their graphs.

3.2 The HBV Model

The Hydrologiska Byråns Vattenbalansavdelning (HBV) model is a conceptual rainfall-runoff model developed by the Swedish Meteorological and Hydrological Institute.The HBV model is designed to predict daily water discharge, relying on daily variations in rainfall, temperature, and potential evaporation. [Seibert, 1996]

It is compartmentalized into different conceptual elements representing snow, soil moisture, and different types of reservoirs for runoff generation. It utilizes a mix of physical parameters and empirical formulas to represent various hydrological processes such as precipitation, snowmelt, evapotranspiration, and runoff. [Seibert, 1996]

3.2.1 Snow Accumulation and Melting

The HBV model differentiates between snow and rain based on a critical temperature threshold, known as the threshold temperature (TT). This critical temperature parameter is crucial in determining whether precipitation will add to the snowpack or contribute to soil moisture and runoff. The model accounts for snow accumulation, which is modified by the snowfall correction factor (SFCF). This factor adjusts the amount of snowfall received, taking into account various local conditions.

Snow melting is a crucial aspect of the model, especially in cold climates or high-altitude regions where snow can constitute a significant portion of the annual precipitation. The melting process is calculated using the degree-day method, which multiplies the degree-day factor (CFMAX) by the difference between the daily temperature (T(t)) and the threshold temperature (TT), see Equation

3. This approach assumes a linear relationship between the amount of melt and the temperature above the threshold.

The model also considers the refreezing of liquid water within the snowpack. This process is especially relevant in environments where temperatures fluctuate around the freezing point. Refreezing is quantified using the refreezing coefficient (CFR) and the degree-day factor (CFMAX), adjusted by the difference between the threshold temperature and the daily temperature.

$$\text{melt} = \text{CFMAX} \times (T(t) - TT) \tag{3}$$

$$\text{refreezing} = \text{CFR} \times \text{CFMAX} \times (TT - T(t)) \tag{4}$$

3.2.2 Soil Moisture and Groundwater Recharge

The model's handling of soil moisture and groundwater recharge is essential for understanding water movement within a catchment. Rainfall and snowmelt, once determined based on the temperature, contribute to these components. The soil moisture content is crucial in determining how much of the incoming water will infiltrate and recharge the groundwater as opposed to contributing to surface runoff.

Soil moisture dynamics are influenced by several factors, including soil properties, vegetation cover, and topography. The model encapsulates this complexity through parameters such as the field capacity (FC) and a soil moisture response factor (BETA), see Equation 5. The field capacity represents the maximum amount of water the soil can hold, and the response factor modulates the soil's ability to absorb water based on its current moisture content.

$$\frac{\text{recharge}}{P(t)} = \left(\frac{\text{SM}(t)}{\text{FC}}\right)^{\text{BETA}} \tag{5}$$

3.2.3 Evapotranspiration

Evapotranspiration is a key process in the hydrological cycle, representing the transfer of water from the land to the atmosphere. In the HBV model, actual evaporation is calculated by considering potential evaporation (E_{pot}) and the current soil moisture status ($\text{SM}(t)$), as well as a scaling factor (LP) typically ranging from 0.5 to 1, as shown in Equation 6. Potential evaporation is the amount of evaporation that would occur under ideal conditions, usually estimated from meteorological data. The model adjusts this value based on the soil moisture content, recognizing that evaporation rates will be lower when the soil is dry.

This component of the model is particularly important in arid or semi-arid regions, where evaporation can significantly reduce water availability. The model's ability to simulate actual evaporation helps in understanding the water balance and predicting streamflow under different weather conditions.

$$E_{\text{act}} = E_{\text{pot}} \times \min\left(\frac{\text{SM}(t)}{\text{FC} \cdot \text{LP}}, 1\right) \tag{6}$$

3.2.4 Groundwater Dynamics

Groundwater dynamics are modeled to represent the slower, subsurface component of the hydrological cycle. This includes the flow of water through different layers of soil and rock, eventually contributing to streamflow. The model incorporates various flow rates (K0, K1, K2) representing different subsurface layers or zones, see Equation 7. These rates are crucial for simulating how groundwater responds to rainfall and snowmelt events, as well as how it sustains baseflow in streams during dry periods.

Understanding groundwater dynamics is essential for long-term water resource management, especially in regions dependent on groundwater for drinking water and irrigation. The HBV model's representation of groundwater helps in predicting how aquifers will respond to different climatic scenarios and land-use changes.

$$\begin{aligned} Q_{\text{GW}}(t) = {} & K_2 \times \text{SLZ} \\ & + K_1 \times \text{SUZ} \\ & + K_0 \times \max(\text{SUZ} - \text{UZL}, 0) \end{aligned} \tag{7}$$

3.2.5 Runoff Simulation

The culmination of the HBV model is the simulation of runoff, which is the water that flows over the land surface and into streams and rivers. This component integrates the effects of precipitation, snowmelt, soil moisture, and groundwater dynamics to simulate the streamflow. Runoff simulation is critical for understanding flood risks, managing water resources, and predicting the impacts of climate change on water availability.
The model uses a time-stepped approach to aggregate the contributions from different processes and storages over time. This allows for the simulation of how streamflow varies in response to weather patterns, seasonal changes, and longer-term climatic trends. The runoff module's outputs are vital for planning and managing water resources in river basins, including reservoir operations, flood forecasting, and ecological conservation efforts.

$$Q_{\text{sim}}(t) = \sum_{i=1}^{\text{MAXBAS}} c(i) \times Q_{\text{GW}}(t - i + 1) \tag{8}$$

Where $c(i) = \int_{i-1}^{i} \frac{2}{\text{MAXBAS}} - \left|u - \frac{\text{MAXBAS}}{2}\right| \times \frac{4}{\text{MAXBAS}^2}\, du.$

3.2.6 Manual Calibration

The HBV light model was initially run with its "out of the box" default parameters, which can be seen

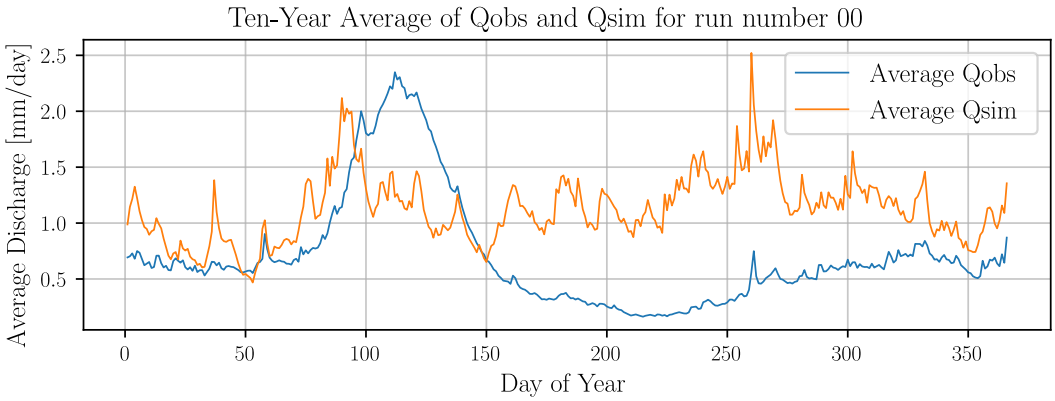

Figure 1: This plot shows the yearly simulated (Qsim in orange) and observed (Qobs in blue) average discharge for the entire data set (1982 to 1991) with the uncalibrated HBV model. The simulated discharge is seen to be substantially discrepant from the observed discharge from approximately day 100 onwards.

in Table 1 in the row for Run 00. These parameters yielded an R_{eff} score of -0.8164 and a mean difference of -152 [mm/year]. Additionally, the ten-year average simulated discharge (Q_{sim}) and observed discharge (Q_{obs}) were plotted against time as seen in Figure 1. Together, these measures indicate that the default model performed very poorly. From Figure 1, we see that the simulated spring-discharge peak, which occurs when all the snow melts, comes earlier than observed. This can be corrected by increasing the critical temperature TT from 0 to 1, essentially indicating that the temperature needs to be higher for the snow to melt. This was the first step in the manual calibration, as seen in Run 01 in Table 1 and in Figure 40 in the Appendix, Section 7. This resulted in an increase of the R_{eff} score to -0.6442 and in the mean difference to -143 [mm/year], a slight improvement. In Run 02, we continued with the snow routine aspects of the model and improved the degree-day factor. This factor controls how fast snow melts to become liquid water, which then contributes to runoff. As seen in Figure 41, the simulated discharge in the spring is abrupt. This slope can be made more gradual by decreasing the CFMAX parameter, which was reduced from 3 to 2. This change resulted in Figure 41 in the Appendix, Section 7. Now that the snow routine is somewhat well-fitted, let us move on to the soil routine. First, let us get a better understanding of how the parameter BETA affects the hydrograph.

By increasing the parameter BETA in Equation 5, the amount of recharge becomes more exponentially proportional to the soil moisture. This means that, for a high value of BETA, when the soil is unsaturated, the amount of recharge is squeezed towards zero and is lower than for a low value of BETA. This effect can be seen in Figure 2. The point at which the ratio of recharge to precipitation reaches 1 is where the soil moisture reaches the field capacity.

Now, looking at the hydrograph in Figure 41, we see that the simulated discharge is too high compared to the observed discharge. This can be improved with the knowledge we have now obtained about the BETA parameter. We want to slow down the amount of discharge that appears after spring, and we can do so by increasing the parameter. Thus, BETA is increased from BETA $= 1$ to BETA $= 4$ as seen in Run 03. This has a major impact on the model efficiency and mean difference. We now have a positive R_{eff} score of 0.1085 and a mean difference equal to -66. The results can also be seen very clearly in the hydrograph plot in Figure 42 in the Appendix, Section 7.

Next, we would like to smooth out the simulated runoff a bit to more closely resemble the observed one. This is done by increasing the MAXBAS parameter, transforming the runoff, and prolonging the time it takes to flow out, making it less abrupt. Thus, MAXBAS is increased from MAXBAS $= 1$ to MAXBAS $= 3$ as seen in Run 04. This increased the R_{eff} score to a value of 0.2391, but the mean difference stayed the same.
The peak flows or the fast runoff component of the upper storage reservoir, $Q0$, have increased too much over the past iterations, and must therefore be tuned. This is done by varying the scaling factor, $K0$, for the fast flow. Thus, for Run 05, $K0$ was decreased from $K0 = 0.2$ to $K0 = 0.02$. This had a substantial impact on the model performance, increasing the R_{eff} score to a value of 0.5229, but again the mean difference stayed the same at -66.

We are slowly but surely getting closer to reaching a good model, as seen in Figure 44. The tuning process above is continued using intuition and understanding of the physical processes in the model. After 17 runs, the model reaches a reasonable efficiency and mean difference of 0.8755 and 12 [mm/year], respectively. The model can obviously be further tuned, but then one risks starting to delve deeper into an overfitting

Table 1: HBV Model Calibration

Run#	ΔP	TT	CFMAX	FC	LP	BETA	PERC	UZL	K0	K1	K2	MAXBAS	R_{eff}	Mean diff.
00		0	3	200	1	1	1	20	0.2	0.1	0.05	1	-0.8164	-152
01	TT	1	⋮	⋮	⋮	⋮	⋮	⋮	⋮	⋮	⋮	⋮	-0.6442	-143
02	CFMAX	1	2	⋮	⋮	⋮	⋮	⋮	⋮	⋮	⋮	⋮	-0.4898	-145
03	BETA	1	2	⋮	⋮	4	⋮	⋮	⋮	⋮	⋮	⋮	0.1085	-66
04	MAXBAS	1	2	⋮	⋮	4	⋮	⋮	⋮	⋮	⋮	3	0.2391	-66
05	K0	1	2	⋮	⋮	4	⋮	⋮	0.02	⋮	⋮	3	0.5229	-66
06	FC	1	2	350	⋮	4	⋮	⋮	0.02	⋮	⋮	3	0.6692	-41
07	PERC	1	2	350	⋮	4	5	⋮	0.02	⋮	⋮	3	0.7577	-41
08	LP	1	2	350	0.8	4	5	⋮	0.02	⋮	⋮	3	0.8217	6
09	CFMAX	1	2.2	350	0.8	4	5	⋮	0.02	⋮	⋮	3	0.8279	7
10	BETA	1	2.2	350	0.8	5	5	⋮	0.02	⋮	⋮	3	0.8511	17
11	CFMAX	1	2.19	350	0.8	5	5	⋮	0.02	⋮	⋮	3	0.8513	17
12	TT	0.96	2.19	350	0.8	5	5	⋮	0.02	⋮	⋮	3	0.8532	16
13	K2	0.96	2.19	350	0.8	5	5	⋮	0.02	⋮	0.056	3	0.8571	16
14	MAXBAS	0.96	2.19	350	0.8	5	5	⋮	0.02	⋮	0.056	1.9	0.8639	16
15	UZL	0.96	2.19	350	0.8	5	5	32	0.02	⋮	0.056	1.9	0.8745	16
16	TT & FC	0.999	2.19	325	0.8	5	5	32	0.02	⋮	0.056	1.9	0.8703	12
17	K1	0.999	2.19	325	0.8	5	5	32	0.02	0.08	0.056	1.9	0.8755	12
		0.999	2.19	325	0.8	5	5	32	0.02	0.08	0.056	1.9	0.8755	12

scenario. The problem of overfitting the data is later considered in Section **??** on the Split-Sample method. The process is therefore stopped here, and the manual model is considered calibrated.

Depending on whether the temperature is above or below the threshold temperature, TT [°C], precipitation is simulated as either rain or snow, respectively. The snow is multiplied by a snowfall correction factor, SFCF [-], which is kept constant at 0.6. As seen in Figure 6, the snowfall follows a yearly cyclical pattern with peaks during winter, reflecting the seasonality essential for accurate hydrological modeling, particularly in snow-dominated regions. The interplay between precipitation and snowfall highlighted in this figure is a key factor in the calibration and validation of the model, influencing runoff and streamflow predictions.

The soil moisture also follows a cyclical yearly pattern with an increasing trend in the fall, reaching a peak during winter, and a decreasing trend during spring, reaching a trough in the summer, as seen in Figure 7. These patterns are inversely proportional to the trends of evaporation, which decreases during fall/winter and increases during spring/summer. The soil moisture and snowpack dynamics depicted in this figure demonstrate the catchment's ability to store and release water, impacting the timing and magnitude of runoff, infiltration, and baseflow.

The total simulated discharge (Qsim) consists of its three partial flows: a fast or peak flow Q0, an intermediate flow Q1, and a baseflow Q2. As seen in Figure 8, the baseflow in purple is the dominating contribution to Qsim, while the intermediate flow is nearly zero and the peak flow is negligible. This indicates that the quickflow component Q0, represented by the fast flow parameter K0, might not be sensitive due to its minimal contribution to the total discharge. The stability of baseflow and variability of interflow and quickflow, which are crucial for understanding the catchment's hydrological response, can inform the parameterization and calibration of the model. This understanding is foundational for the parameter sensitivity study that follows using the Monte Carlo method in Section 3.2.8, highlighting the significance of each flow component in the model's predictive accuracy.
These observations of hydrological components and their temporal patterns set the stage for a nuanced approach to tuning the model parameters to achieve an accurate representation of the catchment's hydrology. It is essential to capture these baseline behaviors accurately before exploring the intricacies of parameter sensitivity to ensure the model's robustness and reliability.

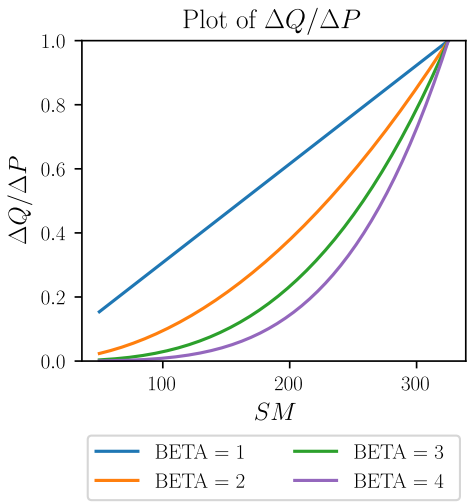

Figure 2: This plot shows the relationship between the change in runoff (ΔQ) per unit change in precipitation (ΔP) and soil moisture (SM) for different BETA values. The horizontal axis quantifies SM content, and the vertical axis represents the dimensionless ratio of runoff to precipitation, which can be interpreted as a measure of the efficiency of precipitation in generating runoff. The four curves correspond to different BETA parameters, where BETA is a non-dimensional factor that modulates the response of runoff to soil moisture changes.

3.2.7 Model Verification - The Split-Sample Method for HBV

In hydrological modeling, the split-sample method serves as a crucial mechanism to validate a model's performance by segregating the available data into two subsets: one for calibration and the other for validation [Arsenault et al., 2018]. This delineation is vital to ensure the model does not overfit to known data, maintaining its generality and predictive accuracy when applied to unseen data [Seibert and Bergström, 2021]. Overfitting undermines a model's robustness, rendering it ineffective in adapting to new or changing conditions. This is particularly critical in a climate change scenario, where models like HBV and WASMOD are employed to project hydrological responses under varying climatic conditions. Through the split-sample method, the model's reliability and adaptability are ascertained, making it a prudent choice for analyzing potential climate-induced hydrological shifts [Seibert and Bergström, 2021][Shen et al., 2022].

Thus, the HBV model was verified by splitting the data set, that in practice span the years 1982 to 1991, in two. The first section (1982 to 1987) is further calibrated using the Run 17 1 form the manual calibration 3.2.6 of the entire data set as an initial ansatz. The calibration method remained the same using intuition, models efficiency and the mean offset to further optimize the model parameters. This yielded the final parameter of the split-sample calibration period as seen in Table 2. They, brought forth an increase in the model efficiency bringing the calibration R_{eff} to 0.8963 compared to the R_{eff} of 0.8755 that was achieved by calibrating on the entire data set. This is as expected and can be attributed to several factors intrinsic to the nature of modeling and data characteristics. One possibility is that the model is in the verge of or actually has been overfitted to the smaller dataset. An other possibility relates to the representativeness and homogeneity of the smaller dataset. The data from 1982 to 1987, which achieved a higher calibration R_{eff} of 0.8963, might be less varied in hydrological characteristics compared to the full dataset spanning 1982 to 1991. This reduced variability can lead to a model that is finely tuned to a specific set of conditions, reflected in its higher efficiency but potentially lacking in broader applicability.

The calibration on the smaller dataset also resulted in a mean difference of 16 mm/year, compared to 4 mm/year for the period 1988 to 1991 Table 3. This larger mean difference suggests that while the model is highly efficient according to R_{eff}, it may not be accurately capturing some of the hydrological processes, possibly due to overfitting or the exclusion of certain hydrological extremes present in the latter period.

Moreover, the reduced complexity required for modeling the smaller dataset could result in a higher R_{eff} due to the model's capacity being more aligned with the reduced data variability. This contrasts with the larger dataset, where the increased complexity needed to account for a broader range of conditions might not be fully realized, leading to a lower R_{eff}.

In light of these observations, the higher R_{eff} achieved with the smaller dataset from 1982 to 1987 should be interpreted with caution. It indicates a good fit for that specific period but does not necessarily imply superior overall model performance, especially when considering the model's ability to generalize across different hydrological conditions and time periods. This highlights the importance of evaluating model performance using diverse metrics and across varied datasets to ensure a comprehensive understanding of its capabilities and limitations.

Table 2: The HBV Model Parameters for the calibration period of the split-sample validation method

Param.	Values	Param.	Values	Param.	Values
TT	1	CFMAX	2.14	FC	310
LP	0.79	BETA	5	PERC	5
ULZ	32	K0	0.02	K1	0.059
K2	0.058	MAXBAS	1.7		

Table 3: Calibration and validation model preformances (R_{eff} score and [mm/year])

Year	1982 - 1987	1988 - 1991
R_{eff}	0.8963	0.8306
Mean diff [mm/year]	16	4

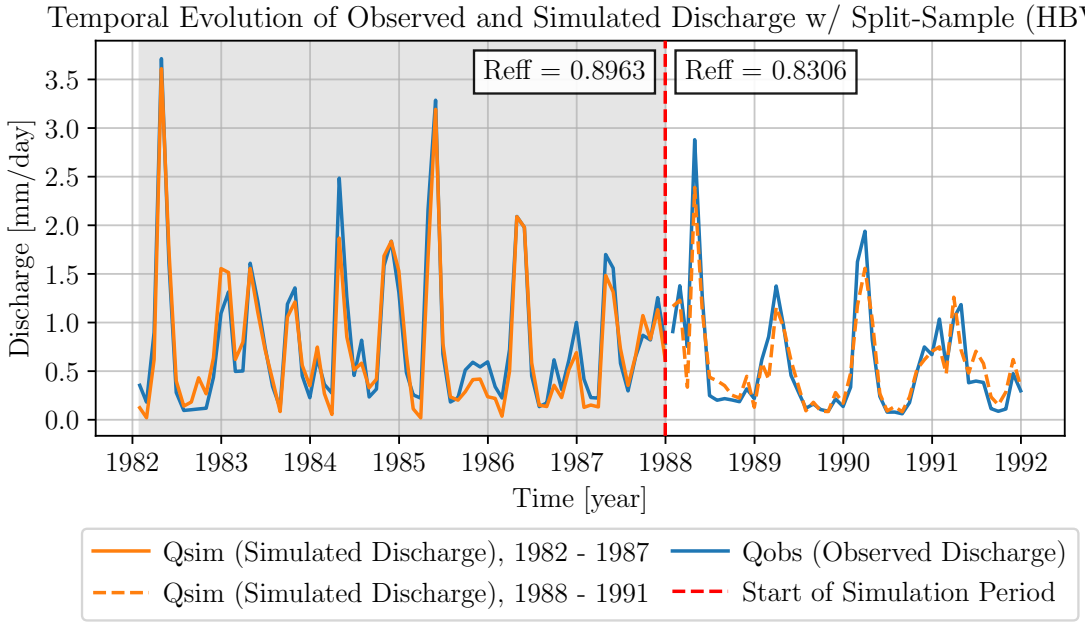

Figure 3: The plot shows the discharge for the calibration period from 1982 to 1987 with gray background and solid orange line on the left of the picture, and the simulated discharge for the verification period from 1988 to 1991 on the right with white background and dached orange line. The intersection of the two periods is plotted in a red-dached line, and on either side of it, in the upper part of the picture, the Reff score for the two periods is shown.

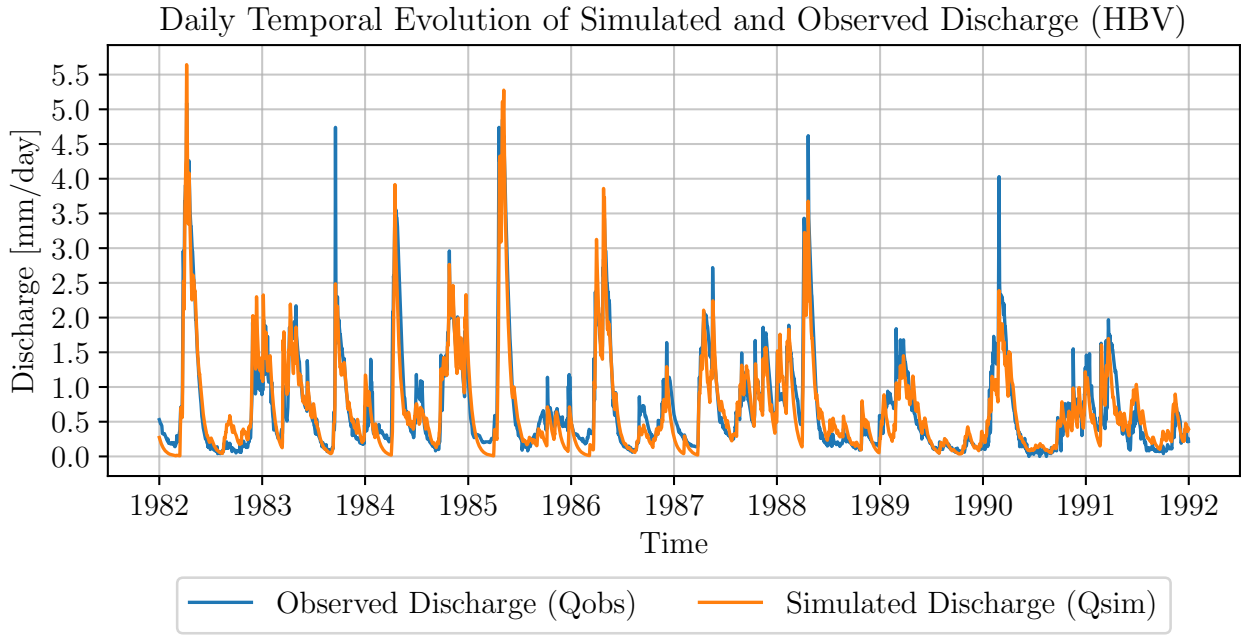

Figure 4: This plot shows the observed (Qobs in blue) and simulated (Qsim in orange) discharge for a daily timestep, using the parameters obtained from Run 17 1 from the manual calibration of the entire data set period (1982 to 1991).

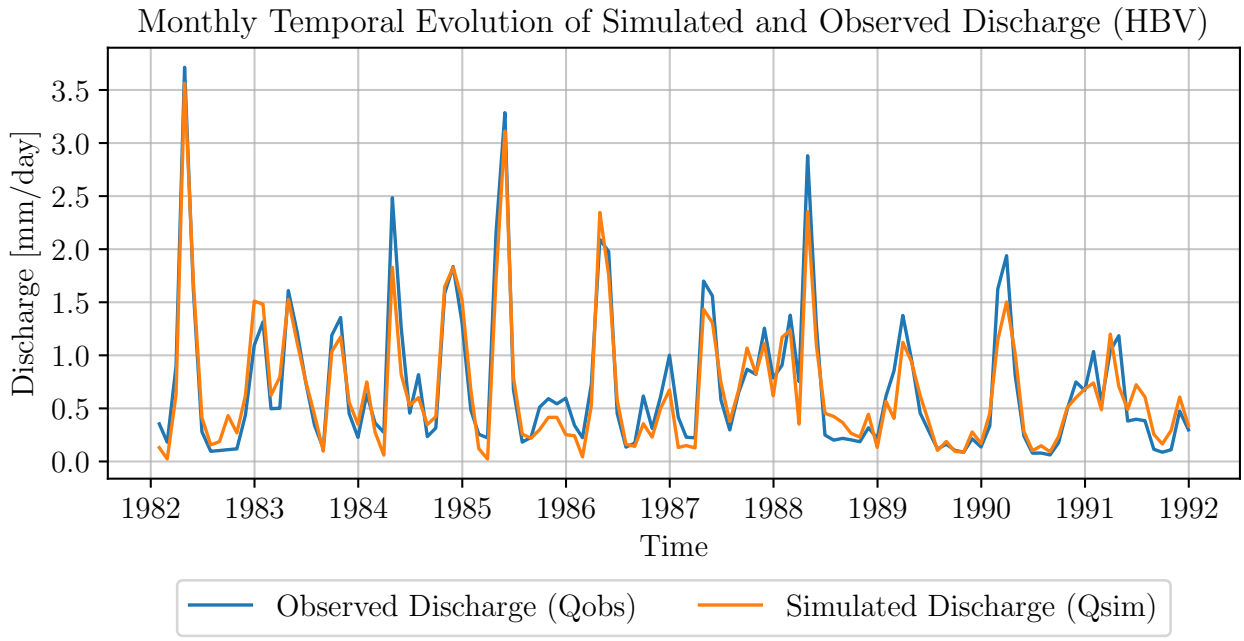

Figure 5: This plot shows the observed (Qobs in blue) and simulated (Qsim in orange) discharge for a monthly timestep, using the parameters obtained from Run 17 1 from the manual calibration of the entire data set period (1982 to 1991).

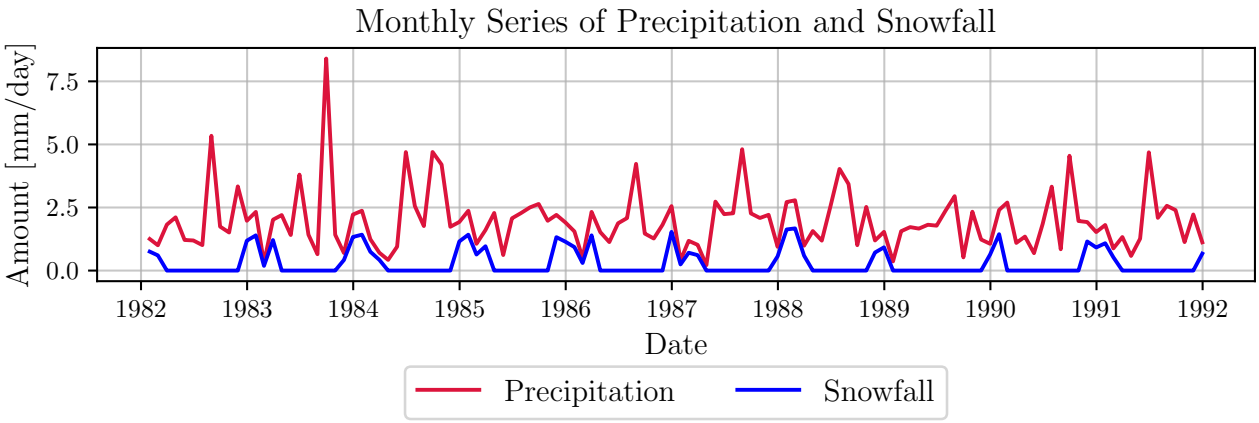

Figure 6: The plot illustrates the monthly series of precipitation and snowfall in mm/day for the specified data period. Precipitation is shown with a red line, while snowfall is indicated by a blue line.

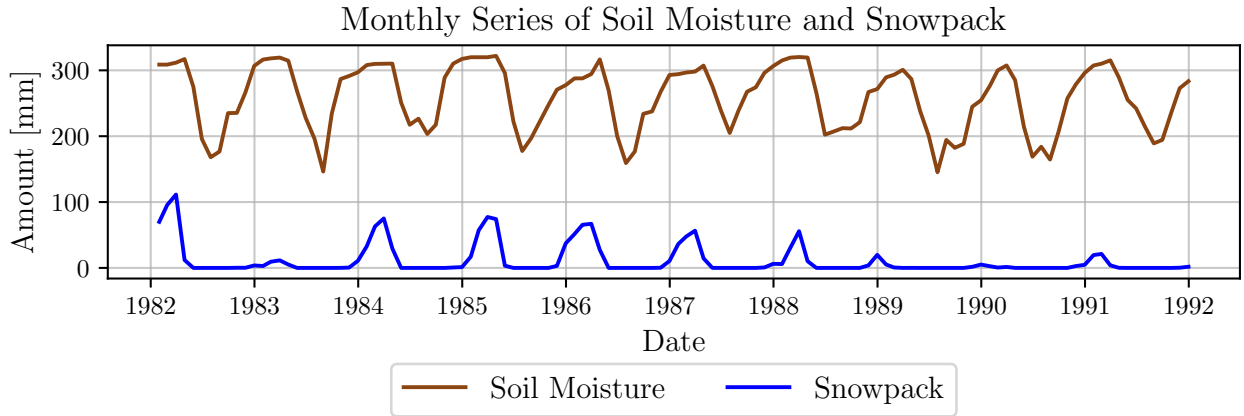

Figure 7: The plot shows the monthly series of soil moisture and snowpack in mm for the specified data period. Soil moisture is depicted with a brown line, while the snowpack is shown with a blue line.

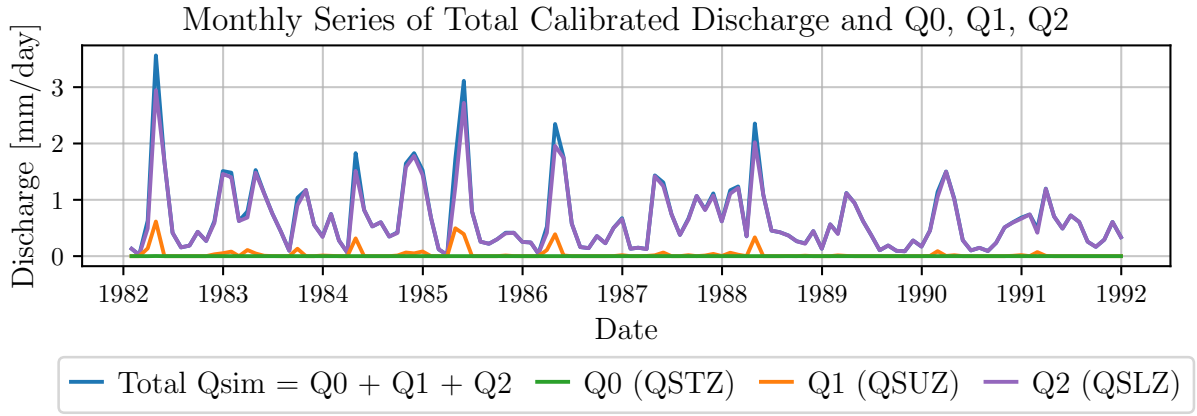

Figure 8: The plot depicts the monthly series of total calibrated discharge (Qsim) in blue for the specified data period, which is the sum of Q0 (baseflow from upper storage, QSTZ) in green, Q1 (interflow from upper storage, QSUZ) in orange, and Q2 (baseflow from lower storage, QSLZ) in purple. The discharge is given in mm/day.

3.2.8 Monte Carlo Calibration

The Monte Carlo option in the HBV light model serves as a tool for conducting sensitivity studies and parameter uncertainty estimations. The Monte Carlo Runs tool allows for multiple model runs with randomly generated parameter sets, facilitating a comprehensive exploration of the model's parameter space.

Therefore, we will now conduct parameter sensitivity studies, first by setting the following ranges for each parameter: TT (-1.5 to 1.5), CFMAX (2 to 5.0), FC (50 to 500), BETA (1 to 4), LP (0.5 to 1), K0 (0.02 to 0.5), K1 (0.02 to 0.50), K2 (0.002 to 0.10), PERC (1 to 5), MAXBAS (1 to 5), UZL (10 to 80), and running 100,000 to 400,000 simulations. In these simulations, parameter values are randomly selected from the ranges. The results from the simulation runs are saved only if their R_{eff} score is greater than 0.7. Note that the parameters CFR, SFCF, CWH, and CET are set to their original values, 0.05, 0.6, 0.1, and 0.1, respectively, and are not changed.

The results show a variety in the sensitivity of the parameters. Some are little sensitive, and their effects on the model performance are minuscule. This can be observed for parameters such as K0, MAXBAS, and PERC in Figures 9, 10, and 11. Particularly for K0, which represents the fast flow component, its minimal impact on model performance may be due to its relatively small contribution to total discharge, as illustrated in Figure 8. This aligns with the observation from Figure 8, where the fast flow component is not prominently featured, suggesting that changes in K0 might not significantly alter the model's output. Such findings challenge our preconceived notions about the influence of certain parameters on model efficacy. Parameters that one might expect to have a significant impact on model performance, like MAXBAS which influences the baseflow, exhibit only minor variations in efficiency within their investigated range. This suggests that the model is relatively robust to changes in these parameters or that other interacting factors may compensate for their variability. Additionally, it highlights the importance of conducting such sensitivity analyses to inform parameter selection, particularly when aiming to generalize the model to different catchments or hydrological conditions.

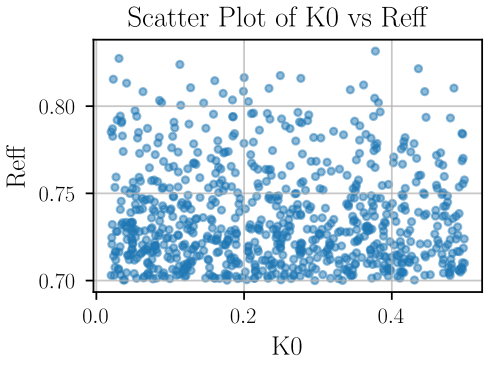

Figure 9: Scatter plot of the parameter K0 againt the model efficiency, for $R_{eff} > 0.7$. The plot shows little variation in efficiency when K0 is altered in the range (0.02 to -0.5).

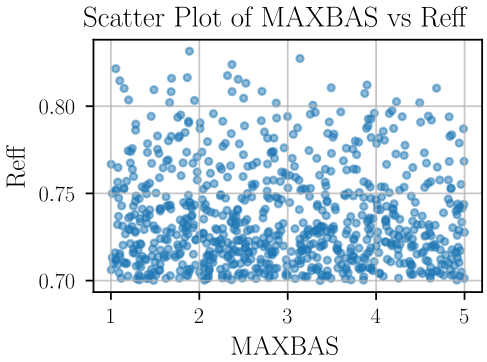

Figure 10: Scatter plot of the parameter MAXBAS againt the model efficiency, for $R_{eff} > 0.7$. The plot shows little variation in efficiency when MAXBAS is altered in the range (1 to 5).

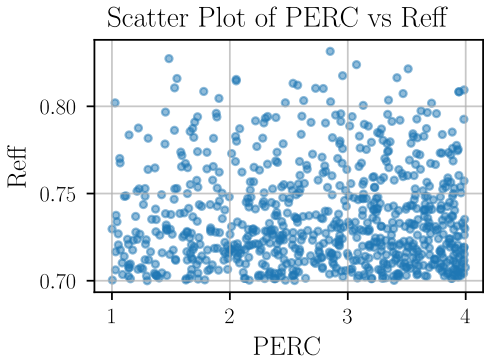

Figure 11: Scatter plot of the parameter PERC againt the model efficiency, for $R_{eff} > 0.7$. The plot shows little variation in efficiency when PERC is altered in the range (1 to 5).

On the other hand, some parameters are more sensitive, and permutations in them have greater implications for the model efficiency. These include, for example, K1, FC, and TT as seen in Figures 12, 13, and 14. The higher sensitivity of these parameters suggests that they play a more pivotal role in the hydrological processes the model simulates. For instance, FC, which affects the field capacity of the soil, shows a marked impact on efficiency, indicating that the model's response to soil moisture capacity is significant. Similarly, TT, the threshold temperature for snowmelt, is also crucial, especially in cold regions where snow processes are dominant. Variations in TT can lead to substantial changes in snowmelt dynamics, affecting runoff and streamflow patterns.

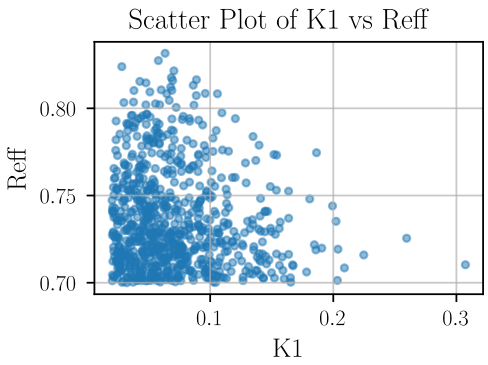

Figure 12: Scatter plot of the parameter K1 against the model efficiency, for $R_{\text{eff}} > 0.7$. The plot shows little variation in efficiency when K1 is altered in the range (0.02 to 0.50).

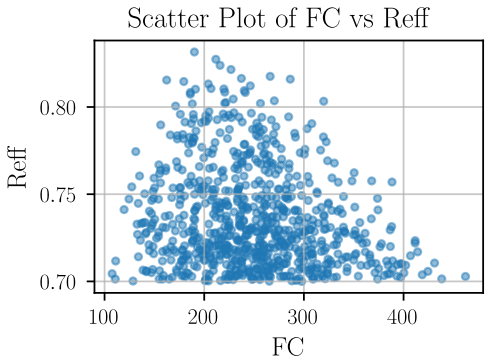

Figure 13: Scatter plot of the parameter FC against the model efficiency, for $R_{\text{eff}} > 0.7$. The plot shows little variation in efficiency when FC is altered in the range (50 to 500).

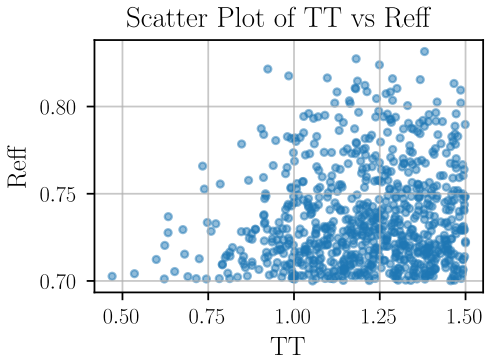

Figure 14: Scatter plot of the parameter TT against the model efficiency, for $R_{\text{eff}} > 0.7$. The plot shows little variation in efficiency when TT is altered in the range (0.02 to 0.50).

3.3 The WASMOD Model

The Water And Snow balance MODelling system (WASMOD) is another conceptual model designed for long-term hydrological simulations. It is primarily used for water balance studies and is based on mass conservation principles. [Xu et al., 2002]

3.3.1 Snow Rutine

The WASMOD's method for calculating snow separation and melting is closer to the degree-day method than to the energy balance method. However, it differs in two ways. First, it uses two threshold temperature parameters, a_1 and a_2, where $a_1 \geq a_2$, instead of e.g. the HBV's degree-day method that only uese one parameter (TT). The snow melting phase begins when the air temperature is higher than a_2 and the snowfall stops when the temperature is higher than a_1. Both snowfall and snowmelting are allowed to take place when temperature is between a_1 and a_2 due to the lumping of time and space [Xu et al., 2002]. Second, the snowmelting during month t is considered a function of temperature and snowpack of that month. For a picture of these

phenonena see Figure 15.
The equation for calculating this snow sheath is

$$sn_t = p_t \left\{ 1 - e^{[(c_t - a_1)/(a_1 - a_2)]^2 \big|} \right\}^+, \quad (9)$$

where sn_t is the snow, p_t is the precipitation, c_t is the current air temperature, and a_1 and a_2 are the model parameters. Note that the $\cdot^+ = max(\cdot, 0)$. This yields the following equation for the actual rainfall r_t

$$r_t = p_t - sn_t. \quad (10)$$

Furthermore, the snoemelt during month t is given by

$$m_t = sp_{t-1} \left\{ 1 - e^{-[(c_t - a_2)/(a_1 - a_2)]^2 \big|} \right\}^+ \quad (11)$$

and is a function of both the temperature c_t and the snowpack at the beginning of the monthsp_{t-1}. Moreover, the snowpack balance is wtitten as

$$sp_t = sp_{t-1} + sn_t - m_t. \quad (12)$$

This is also depicted in Figure 15.

3.3.2 Computation of evapotranspiration

The actual evapotranspiration e_t depends on several factors, but the two that were considered the most important by [Xu et al., 2002] are the monthly potential evapotranspiration ep_t and the available water w_t during the current month. The value of w_t is difined as

$$w_t = r_t + sm_{t-1}^+ \quad (13)$$

where $sm_{t-1}^+ = max(sm_{t-1}, 0)$ is the available water storage.
But, first the long-term average monthly potential evapotranspiration data is adjusted using the following equation

$$ep_t = (1 + a_3 (c_t - \bar{c}))\, \overline{ep}. \quad (14)$$

Here, ep_t is the adjusted monthly potential evapotranspiration, a_3 is a model parameter, c_t is still monthly mean air temperature, $\bar{c}$ is the monthly long-term average temperature in deg C and $\overline{ep}$ is the monthly long-term average values of potential evapotranspiration.
Then the actual evapotranspiration e_t is calculated either as

$$\begin{aligned} e_t &= \min \left\{ ep_t \left(1 - {a_4}^{W_t / \max(ep_t, 1)} \right), w_t \right\} \text{ or} \\ e_t &= \min \left\{ w_t \left(1 - e^{-a_4 ep_t} \right), ep_t \right\} \end{aligned} \quad (15)$$

depending on if we have energy or storage dependent evaporation.

3.3.3 Computation of slow flow component

The slow flow is essentially probortional to the storage in the catchment during that month. Thus, it is given by

$$s_t = a_5 (sm_{t-1}^+)^{b_1}. \quad (16)$$

Here, a_5 and b_1 are non-negative parameters, but as adressed in [Xu et al., 2002] b_1 is set to be a descreate parameter set to equal the values 1 or 2 (in some cases 0 or 1/2), due to its high correlarity with the continous model parameter a_5.

3.3.4 Computation of fast flow component

The fast flow is given by

$$f_t = a_6 \left(sm_{t-1}^+ \right)^{b_2} n_t, \quad (17)$$

where a_6 and b_2 are non-negative parameter, and $n_t = p_t - ep_t \left(1 - e^{-p_t / \max(ep_t, 1)} \right)$ is "active" rainfall. Here, as in the case above, b_2 takes the values 1 or 2.

3.3.5 Computation of total runoff and water balance

Thus, the total runoff is given by

$$d_t = s_t + f_t, \quad (18)$$

and the water balance equation for the soil moisture storage at the end of month t is given by

$$sm_t = sm_{t-1} + p_t - r_t - d_t. \quad (19)$$

3.3.6 Parameter interpretation

3.4 Model Initialisation

The binary parameters b_1 and b_2 together with the two possabilitis for the evapotranspiration Equations 15 grant $2 \times 2 \times 2 = 8$ model combinations. The optimum model for a given catchment is manually selected after all 8 models are run in the calibration part of the WASMOD.exe script. The script was calibrated using the "preliminary run" option on the whole obervation period (1982 - 1991) and the following results were brought forth in the execution window

Table 4: Summary of Calibration Results

Model	IE	B1	B2	R^2	#S	NO	NSI
(1)	1	1.	1.	.812	0	0	0
(2)	1	1.	2.	.843	0	0	0
(3)	1	2.	1.	.831	0	0	0
(4)	1	2.	2.	.849	0	0	0
(5)	2	1.	1.	.819	1	0	0
(6)	2	1.	2.	.848	0	0	0
(7)	2	2.	1.	.833	0	0	0
(8)	2	2.	2.	.850	0	0	0

Model = No. of model versions
IE = Choice of the 2 evapotranspiration eqns.
B1 = Choice of slow flow eqns.
B2 = Choice of fast flow eqns.
R^2 = Quality measure (the R^2 value)
#S = No. of seasons with significant residual
NO = No. of non-optimized parameters
NSI = No. of non-significant parameters
The best model for a given catchment is the one with

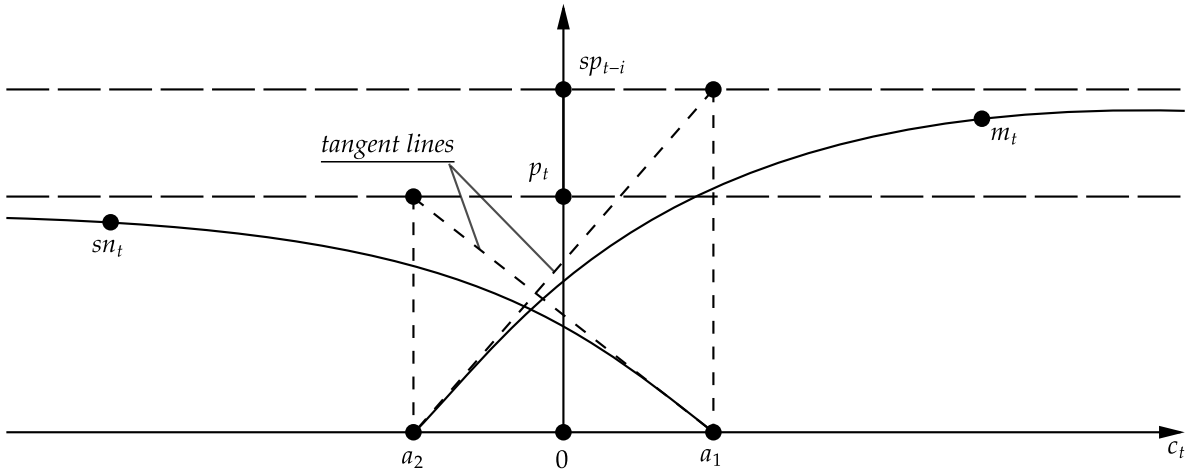

Figure 15: This is a reconstruction of Fig. 2 in [Xu et al., 2002]. It shows the snowfall sn_t and melting m_t during month t as a function of temperature c_t.

the highest R^2 value, lowest #S value, NO = 0, and NSI = 0 or the lowest. Which, for this case is the model number 8 with $b_1 = b_2 = 2$ and using the second evapotranspiration equation in 15 as seen in Table 4. Therefore, this is the model used in the "final run" option, see Figure **??**, and henceforth.

The initial parameter values for the "final run" together with the optimum parameters obtained form that run can be seen in Table 5. Evolution of the parameters during the iterative model traning can be seen in Figure 25. The figure shows that all the parameters have reached a stable value perhaps already after approximetly 40 iterations, but that the iterative calibration prosess continued passed 100 iterations till it terminated. Additionally, the sum of squares (SSQ) of the residual versus parameter values in the neighborhood of the optimised parameter values is plottet in Figure 26. Here SSQ is equal to

$$SSQ = sum_t\left(\sqrt{q_t} - \sqrt{d_t}\right)^2, \tag{20}$$

where q_t is the observed monthly discharge for month t and d_t is the computed monthly discharge for the same month. The square root of the discharges was found by, [Xu, 1992], [Vandewiele et al., 1992] and [Vandewiele et al., 1993], to be a good way to model such monthly discharges. Similarly, the terms could be squared or taken the log transformation of to emphasise the flow peaks and valleys, respectively.

The parameter values that minimise this residual are also plotted with an × and represent the optimum parameters. These can slo be seen in Table 5. The correlation matrix seen in Figure 16 provides insightful details into the relationships among the WASMOD parameters A(1) through A(6). The strong negative correlation between A(1) (upper threshold temperature for snow processes) and A(2) (lower threshold temperature) at -0.6197 suggests an inverse relationship in temperature regulation for snowfall and melting. This indicates that adjustments in one threshold are often counterbalanced by changes in the other, reflecting the model's sensitivity to temperature variations affecting snow dynamics.

Table 5: Inital, optimised and hypersurface minimal values for WASMOD parameters.

	$A(1)$	$A(2)$	$A(3)$	$A(4)$	$A(5)$	$A(6)$
Initial	.2500	.2300	.6000	.5600	.0510	.2600
Optimum	.3033	-.1419	.1246	.5814	.2498	.1084
Hypersurf. min	0.3030	-.1420	.1250	.5810	.2500	.1080

Parameters A(4), A(5), and A(6), which govern evapotranspiration, base flow, and fast flow, respectively, show significant positive correlations. The correlation between A(4) and A(6) (0.4742) and A(5) and A(6) (0.4587) implies that changes in soil moisture and evaporation rates (A(4)) are closely linked with both the base flow (A(5)) and the rapid runoff processes (A(6)). This correlation signifies the model's depiction of the complex dynamics among evaporation, soil moisture, and runoff.

A(3), with its distinct role in converting average potential evapotranspiration to actual values, exhibits low correlations with other parameters, highlighting its relatively isolated influence in the model.

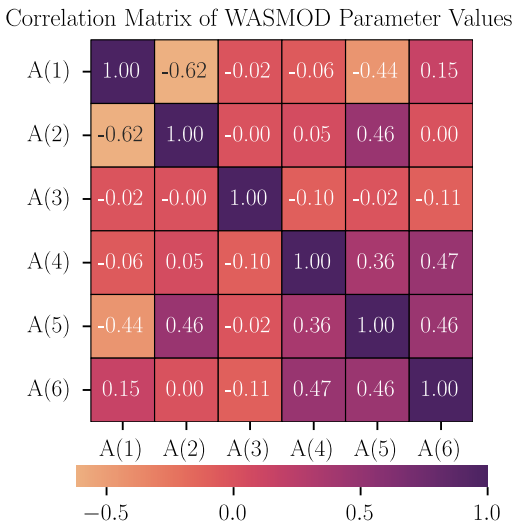

Figure 16: Correlation Matrix of WASMOD Parameters A(1) through A(6). This matrix visually represents the pairwise correlation coefficients between each pair of parameters. A correlation coefficient close to 1 indicates a strong positive correlation, while a value close to -1 indicates a strong negative correlation. Coefficients near 0 suggest little to no linear relationship between the parameters. The color intensity and the sign of each coefficient (positive or negative) are indicative of the strength and direction of the correlation.

3.4.1 Model Verification - The Split-Sample Method

The model preformace was verifide using the split-sample method with the "calibration and simulation" option in the WASMOD executable with model number 8. The model was first calibrated on the data series for the years 1982 till 1987. The optimum parameters obtained for this period were then used to simulate the second period form 1988 till 1991.

As excepted there is a drop in the Reff score for the simulated period compared to the calibration as seen in Figure 17. This is trivial and is due to the natural differences in the metrological atributes of the two periods. However, explaining exactly where these model inacuresis in the simulation periods are is a bit more chalenging.
The convertion of units in the y-axis was done to make it easier to compare the results from the HBV.

As seen in Table 6, the optimised parameter values for the calibration period of the split-sample method, covering 1982 to 1987, exhibit notable differences from those obtained when the model was run over the entire period from 1982 to 1991. This variation in parameter values underscores the sensitivity of the WASMOD model to the temporal scope of the dataset used for calibration.

Focusing on the specific parameters, Parameter A(1), which governs the upper threshold temperature for snow processes, shows an increase from .3033 in the full period to .3264 in the shorter period. This alteration suggests a shift in the temperature range influencing snowfall and melting, indicative of potentially warmer conditions during the earlier years. Parameter A(2), related to the lower threshold temperature for snowfall and melting, also exhibits a change, decreasing from -.1419 to -.1196. This slight increase in value may imply a reduction in the extremity of lower temperature thresholds between the two periods, possibly reflecting a less pronounced temperature variation impacting snow processes.

Parameter A(3) experiences a minor increase from .1246 to .1293, indicating a nuanced adjustment in converting long-term average potential evapotranspiration to actual values. This change could be attributed to minor variations in evapotranspiration conditions, potentially influenced by fluctuating weather patterns across the two periods.

The optimised value of Parameter A(4) decreases from .5814 to .4857, indicating a reduction in the evaporation losses at all moisture storage states during the earlier period. This reduction could be a response to differences in ambient moisture or temperature conditions, impacting the water loss through evaporation.

For Parameter A(5), which influences the proportion of runoff appearing as 'base flow', there is a decrease from .2498 in the full period to .2020 in the shorter period. This decrease suggests a lower proportion of base flow in the earlier period, potentially reflecting variations in catchment storage capabilities or soil properties.

Lastly, Parameter A(6), which determines the fast flow component, shows a reduction from .1084 to .0955. This decrease hints at a slight diminishment in the model's simulation of rapid runoff processes, which could be attributed to differences in rainfall intensity, snowmelt dynamics, and basin conditions between the two periods.

Table 6: Inital parameter values, optimised values calibrated on the entire data series (1982 - 1991) and optimised values calibrated on the first period of the data series (1982 - 1987).

	$A(1)$	$A(2)$	$A(3)$	$A(4)$	$A(5)$	$A(6)$
Initial	.2500	.2300	.6000	.5600	.0510	.2600
Optimum 82-91	.3033	-.1419	.1246	.5814	.2498	.1084
Optimum 82-87	.3264	-.1196	.1293	.4857	.2020	.0955

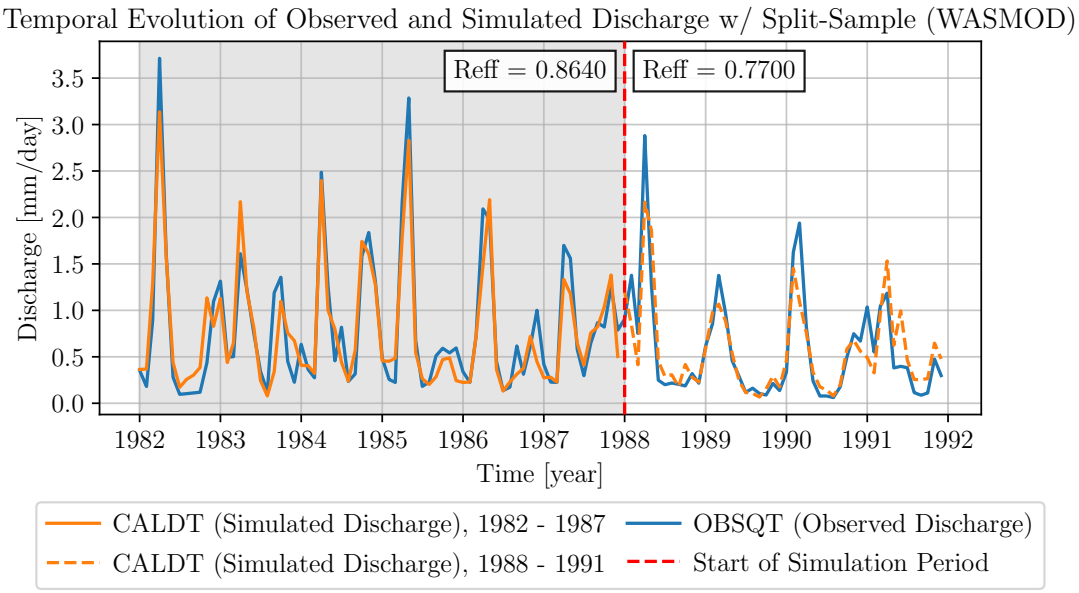

Figure 17: The plot shows the discharge for the calibration period from 1982 till 1987 with gray background and solid orange line on the left of the picture, and the simulated discharge for the verification period from 1988 till 1991 on the right with white background and dached orange line. The intersection of the two periods is plotted in a red-dached line, and on either side of it, in the upper part of the picture, the Reff score for the two periods is shown. Note that the units for the y-axis are in [mm/day] and not in [mm/month].

3.4.2 Further Analysis - The Monte Carlo method

A similar prosidure for estimating the sensitivity and uncertainty of the model parameters as was done for the HBV is also done for the WASMOD. This sensitivity study is done using the Monte Carlo method where the model is given a range for each parameter and a random compination of values are selected and used in the model. The intervals are given by a 2 sigma lower and upper confidence limits around the optimal parameter values found priviously, Table 7.

Analyzing the scatter plots for WASMOD parameters A1 through A6 against model efficiency (R2), we discern the distinct sensitivity and uncertainty characteristics of each parameter.

Table 7: Ranges and Scale of Parameters

Param.	Ranges	Scale
$A(1)$	[0.15, 0.43]	0.1
$A(2)$	[-0.25, 0.0]	0.1
$A(3)$	[0.01, 0.25]	1.0
$A(4)$	[0.25,0.8]	1.0
$A(5)$	[0.08,0.6]	1000.0
$A(6)$	[0.06,0.3]	10000.0

Parameter A1's distribution, peaking at 0.3045, underscores a moderate sensitivity, with model efficiency being responsive within a specific range of values. This indicates that the model's snow processes are finely tuned to the temperature thresholds represented by A1. A2 presents a similar pattern, with the highest R2 at -0.1383, suggesting an optimal lower temperature limit for accurate snow process simulation.
A3 displays a broad distribution of R2 values, converging towards 0.1348. This implies that while the model is somewhat resilient to fluctuations in A3, there is an optimal value for converting long-term evapotranspiration averages to actual values, which does not drastically influence model efficiency.

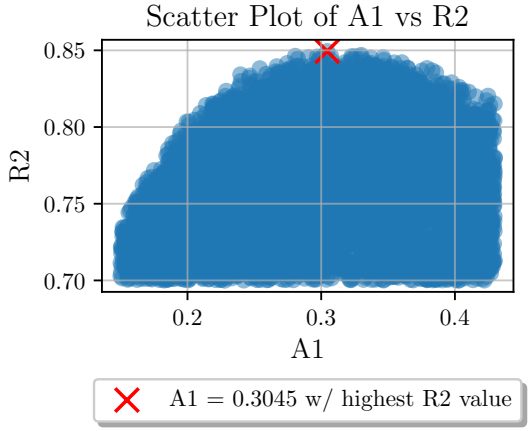

Figure 18: The plot shows how parameter A1 affects the model efficiency. The highest efficiency is marked by an 'X' at A1 = 0.3045, indicating the optimal parameter setting within the tested range.

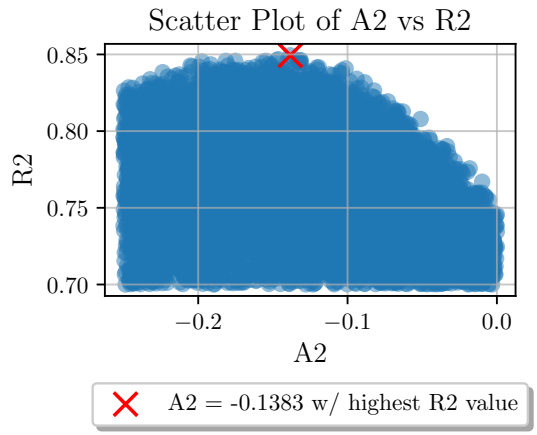

Figure 19: The plot illustrates the relationship between parameter A2 and model efficiency R2. The peak efficiency occurs at A2 = -0.1383, as identified by the 'X', suggesting an optimal lower temperature threshold

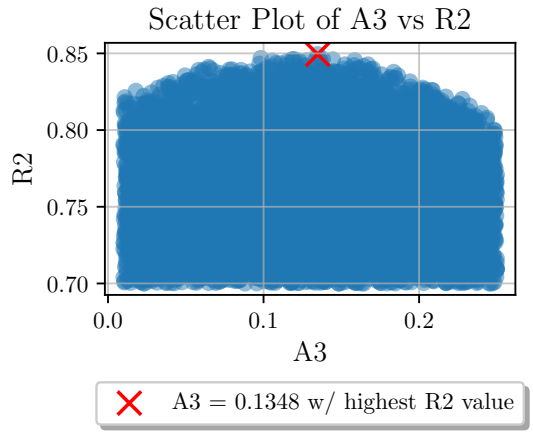

Figure 20: The figure depicts the scatter plot for parameter A3 against R2. The optimal value for A3 is shown at 0.1348 where the model reaches its highest efficiency.

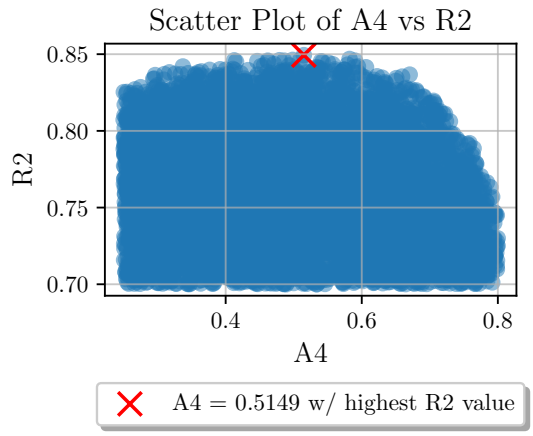

Figure 21: The plot presents the sensitivity of the model efficiency R2 to parameter A4. A clear trend toward higher efficiency is observed, with the highest R2 at A4 = 0.5149.

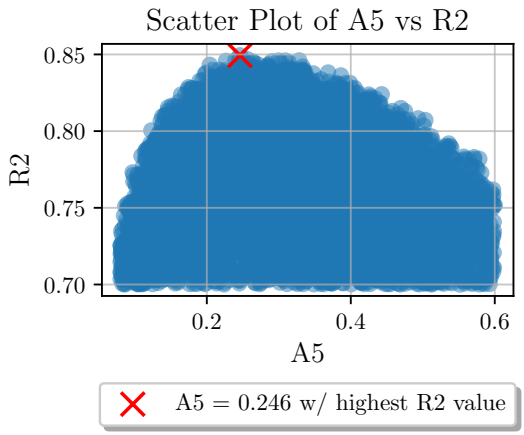

Figure 22: The plot shows the influence of parameter A5 on the model's R2. The 'X' marks the highest model efficiency at A5 = 0.246, indicating the importance of base flow calibration.

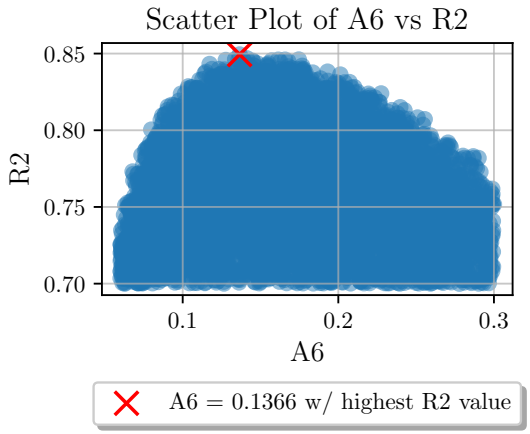

Figure 23: The plot maps the relationship between parameter A6 and R2. The model's efficiency is highest at A6 = 0.1366, marked by 'X', emphasizing the sensitivity of the fast flow response to this parameter

A notable sensitivity to A4 is observed, with a clear gradient of increasing R2 values, peaking at 0.5149. This indicates that the model's evapotranspiration is significantly affected by this parameter, and precise calibration is required for optimal model performance. A5's peak at 0.246 reveals that the base flow component of the model, while sensitive, has an identifiable range where the model operates with the highest efficiency. This suggests that the storage and slow response components of the watershed represented by A5 are critical to the model's accuracy.
Lastly, A6 shows a distinct sensitivity, akin to A4, with the highest R2 at 0.1366. This highlights that the model's fast flow response is sensitive to changes in this parameter, implying that accurate representation of rapid runoff processes is vital for model reliability.

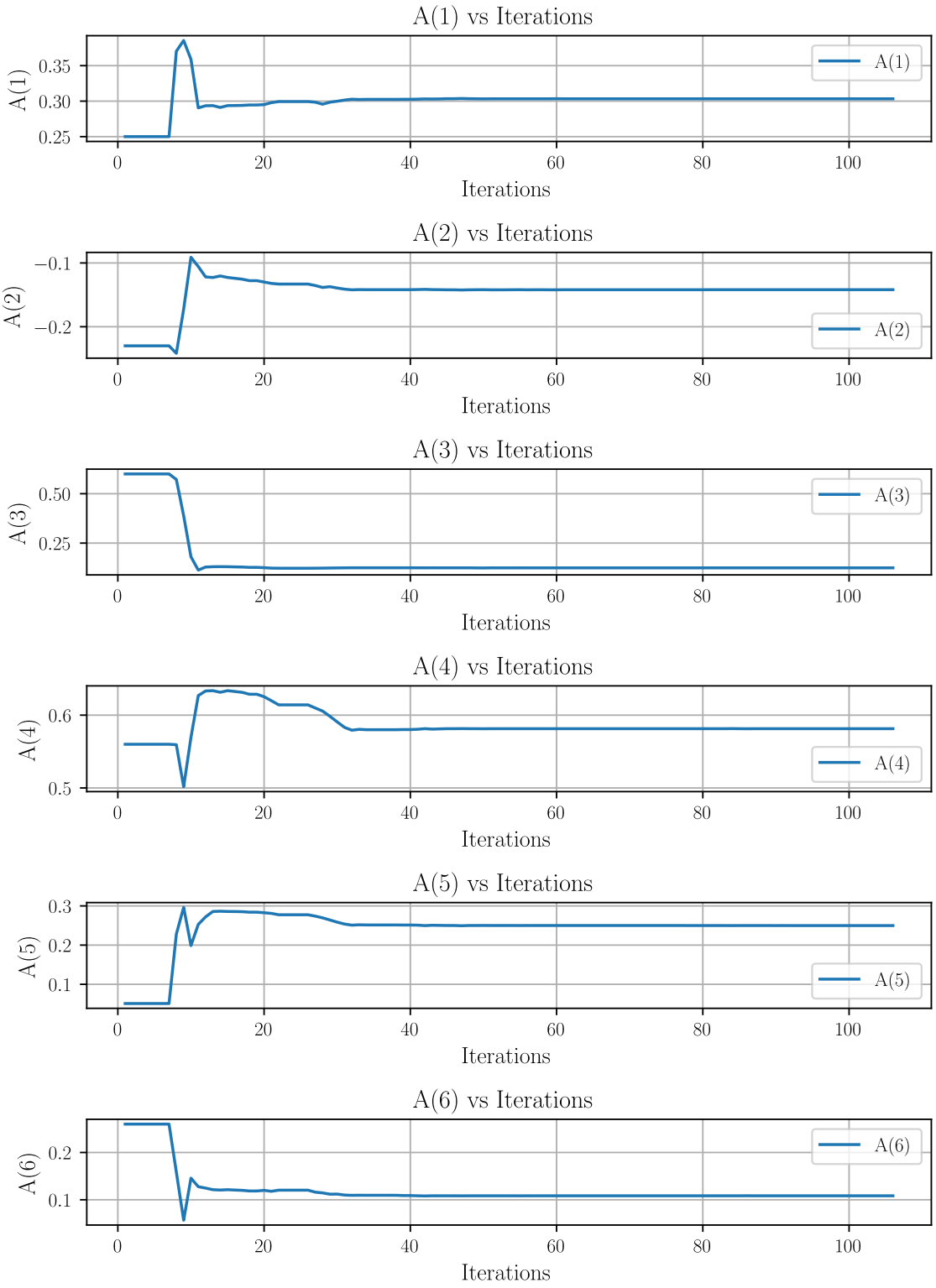

Figure 25: The figure shows the parameter values plotted against the number of iterations. We see that the parameters have just about stabilized allready after 40 iterations, but that the model runs past 100 iterations until it is satisfied with their convergence. The optimization prosess is then terminated and the model is considered optimized.

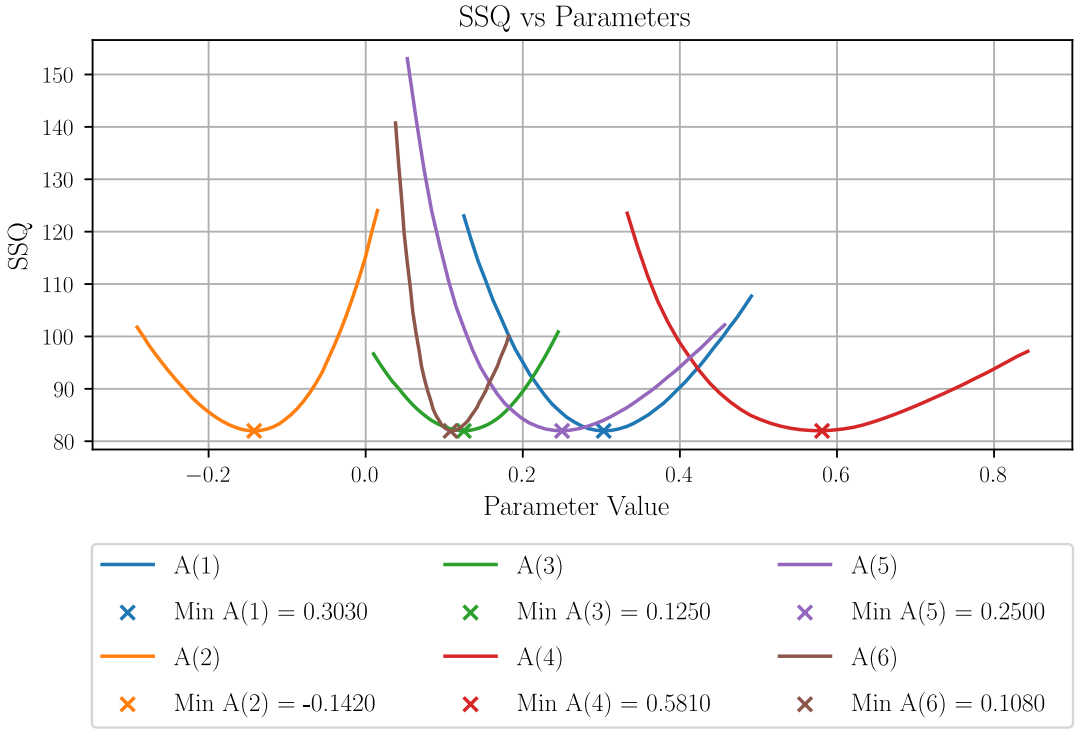

Figure 26: The plot shows the sum of squares (SSQ) of the residual versus parameter values in the neighborhood of the optimised parameter values. Additionally, the parameter values that minimise this residual are also plotted with an × and represent the optimum parameters. The spread or opening of the parabulas describe how sensitive the different parameters are to permutations, e.g. when comparing the parameter A(4) in red with A(6) in brown one sees that A(4) has a wide spread thus being less sensitive than A(6) which has a narrower spread.

3.5 Evaluation and Comparison of the Two Models

Now, that the two models have been calibrated and verified individually we can move ahead and evaluate and compare their preformances to eachother.

As observed in Figure 27 both the HBV and WASMOD are capable of reproduceing historical monthly discharge with little differences in their results. This happens even though the models have discrepancies in how they model evapotranspiration and snowpack, as seen in Fugure 28 and 29, respectively. Note the substantial difference in the snowpack modelled by the two models. The fact that the models are able to reproduce historical discharge with high accuracy while at the same time model the physical prossesis, i.e. evapotranspiration and the forming of the snowpack, so differently may indicate that the relation between the prossesis are not unique. This is one example of a type of equifinality [Her and Seong, 2018].

3.6 Determination of Climate Change Scenarios

3.6.1 Scenario 1: $\Delta T = +3C$, $\Delta P = 0\%$

In the first scenario the temperature was increased by three degrees Celcius in the model input files, ptq.txt and iswedwn.txt. This is done using a simple Python script that reads in the files, adds three degrees to the temperature column, and writes out the file again.

3.6.2 Scenario 2: $\Delta T = +3C$, $\Delta P = +15\%$

Similarly, the input files were updated in scenario 2 by adding three degrees Celcius to the temperature column and multiplying the precipitation column by 1.15, increasing it by 15%.

3.6.3 Scenario 3: $\Delta T = +3C$, $\Delta P = -15\%$

Lastly, the files were updated for the third scenario like they were for scenario 2 accsept that precipitation column was multiplied by 0.85 decreasing the precipitation by 15%.

4 Results

In the discharge plots (Figures 30, 31, and 32), a consistent leftward shift in peak flows is observed across all three scenarios. This shift is most pronounced in Scenario 3 ($\Delta P = -15\%$), somewhat less evident in Scenario 1 (with no change in precipitation), and least pronounced in Scenario 2 ($\Delta P = +15\%$).

Additionally, a reduction in peak discharge magnitudes is noted in all scenarios, following a similar trend as the temporal shifts. Both HBV and WASMOD models exhibit these changes, though with discernible differences. For instance, WASMOD displays higher peaks in certain years (e.g., spring of 1982, 1984, 1985, and 1986) compared to HBV. Notably, a distinct double peak is observed in 1984 for WASMOD, diverging from the single peak pattern of HBV, which more closely mirrors the historical data. Moreover, a rightward shift in discharge is notable for WASMOD in the years 1984 and 1987.

Concerning evapotranspiration, as depicted in Figures 33, 34, and 35, the WASMOD model shows a marked increase in peak values compared to historical data across all scenarios. In contrast, the HBV model's outputs appear relatively unaffected by the climatic changes.

Finally, the snowpack analysis, based on average values, reveals significant discrepancies between the models and across all scenarios. Both models simulate a substantial reduction in snowpack peaks under altered climatic conditions, compared to the simulations using historical data. The decline in snowpack is particularly noteworthy for WASMOD, whose historical data indicated higher levels than HBV's. Conversely, HBV's simulated snowpack levels nearly diminish to zero in most years (except 1982, 1985, and 1987), reflecting a drastic response to the climate change scenarios.

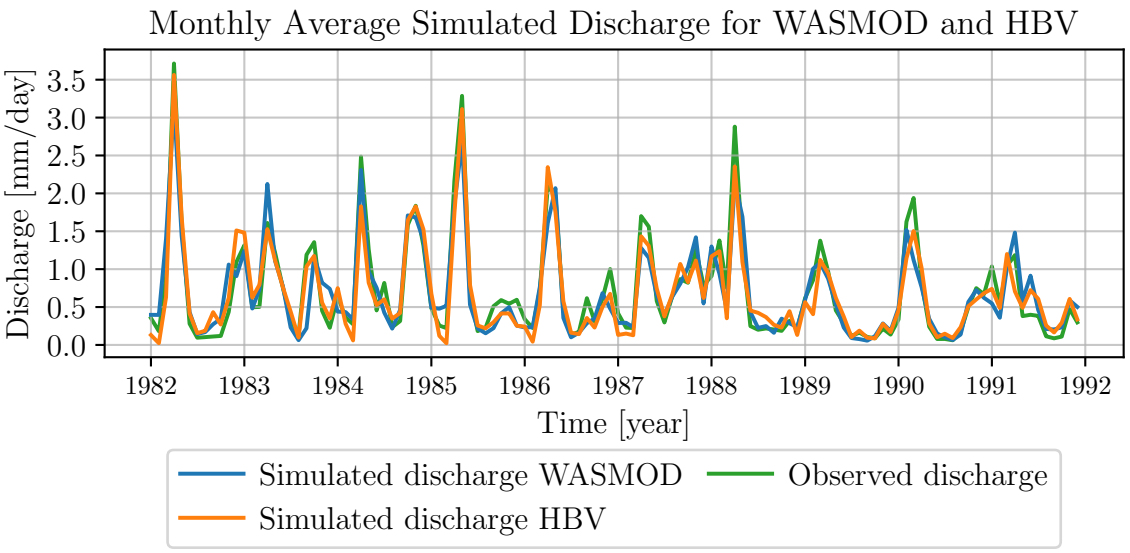

Figure 27: The plot shows the monthly average simulated discharge for the HBV in orange, WASMOD in blue, and the observed monthly discharge in green.

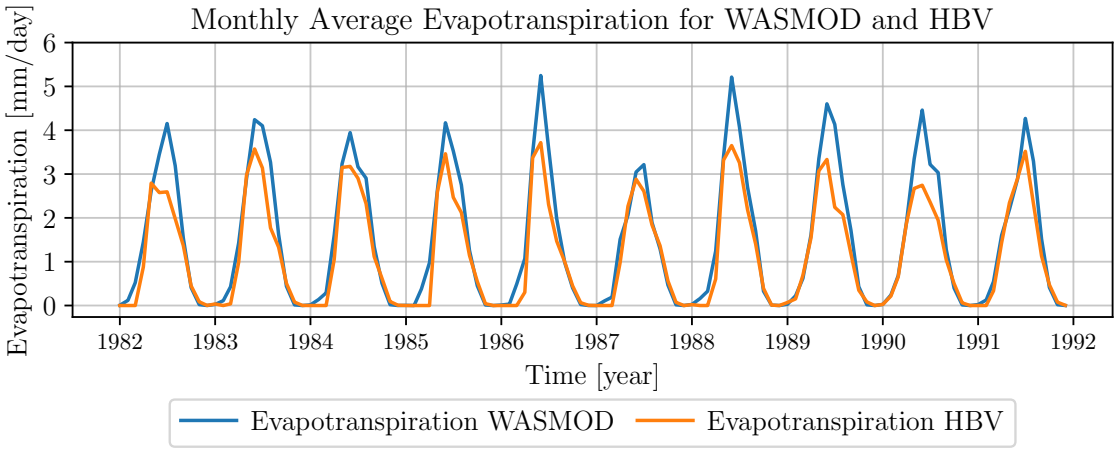

Figure 28: The plot shows the monthly average evapotranspiration for the HBV in orange, WASMOD in blue.

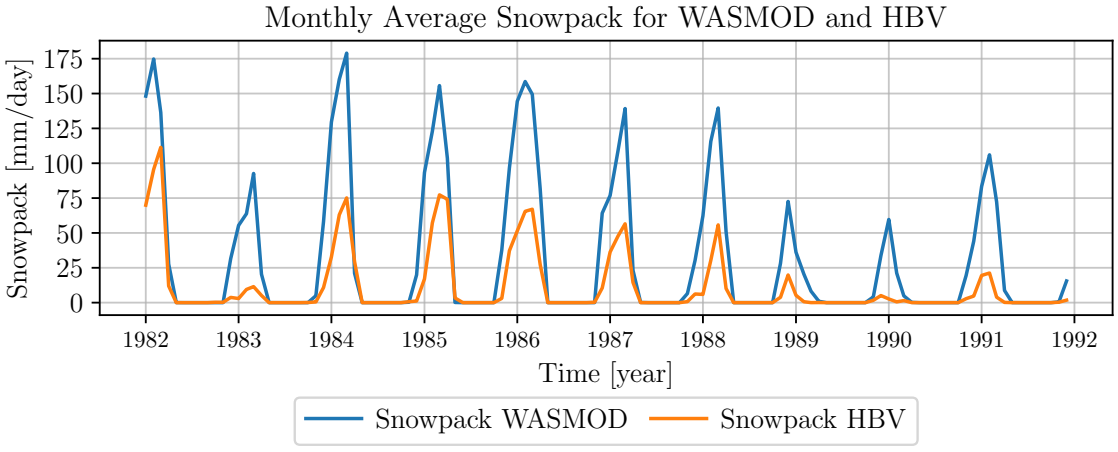

Figure 29: The plot shows the monthly average snowpack for the HBV in orange, WASMOD in blue.

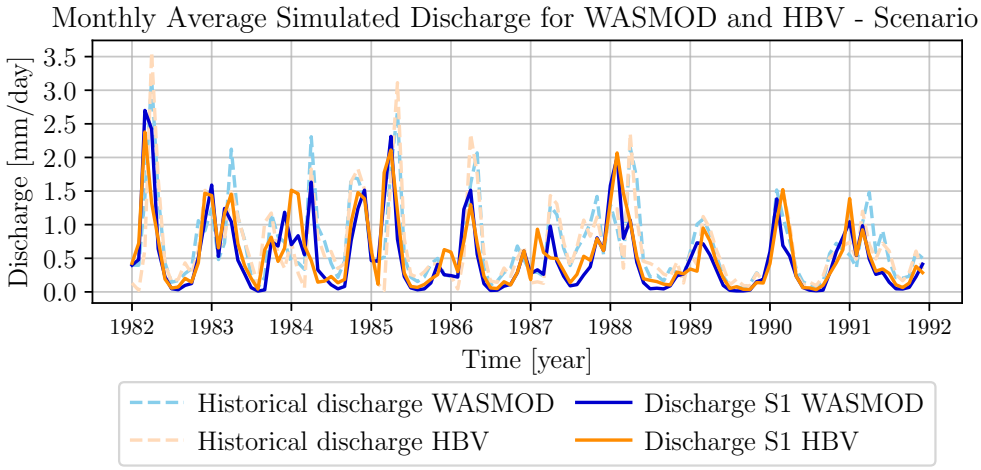

Figure 30: The plot shows the monthly average simulated discharge for the WASMOD in blue and HBV in orange for the first scenario with an increase in temperature $\Delta T = +3C$ and no change in precipitation $\Delta P = 0\%$.

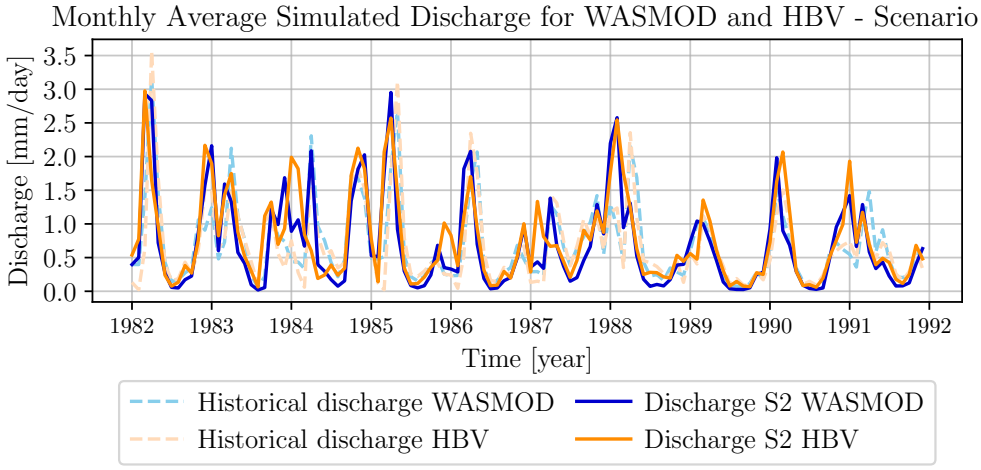

Figure 31: The plot shows the monthly average simulated discharge for the WASMOD in blue and HBV in orange for the second scenario with an increase in temperature $\Delta T = +3C$ and an increase in precipitation $\Delta P = +15\%$.

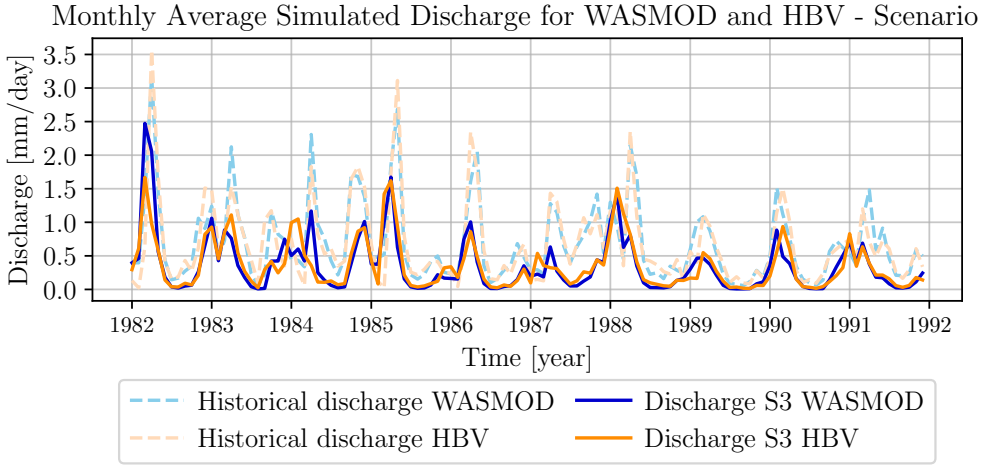

Figure 32: The plot shows the monthly average simulated discharge for the WASMOD in blue and HBV in orange for the third scenario with an increase in temperature $\Delta T = +3C$ and an decrease in precipitation $\Delta P = -15\%$.

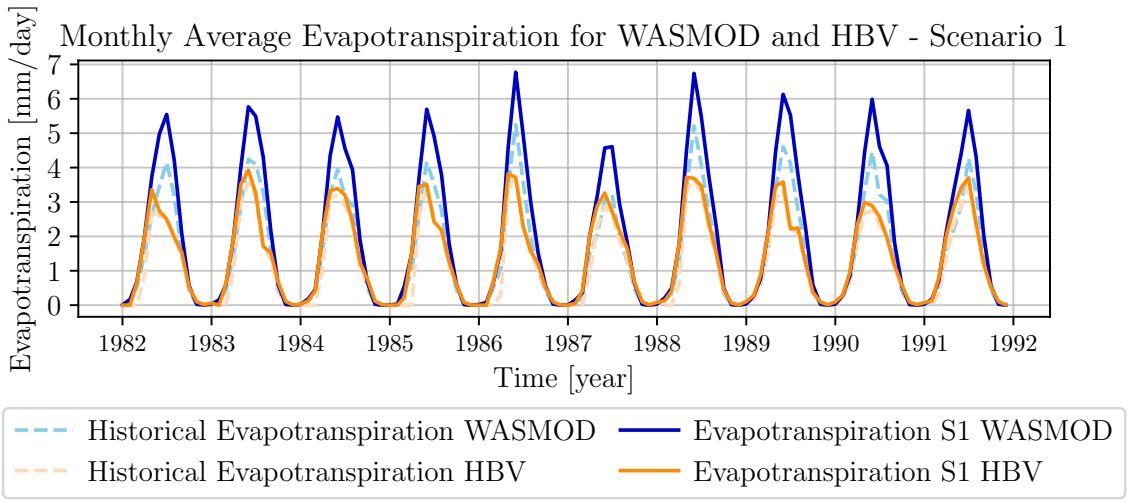

Figure 33: The plot shows the monthly average evapotranspiration for the WASMOD in blue and HBV in orange for the first scenario with an increase in temperature $\Delta T = +3C$ and no change in precipitation $\Delta P = 0\%$.

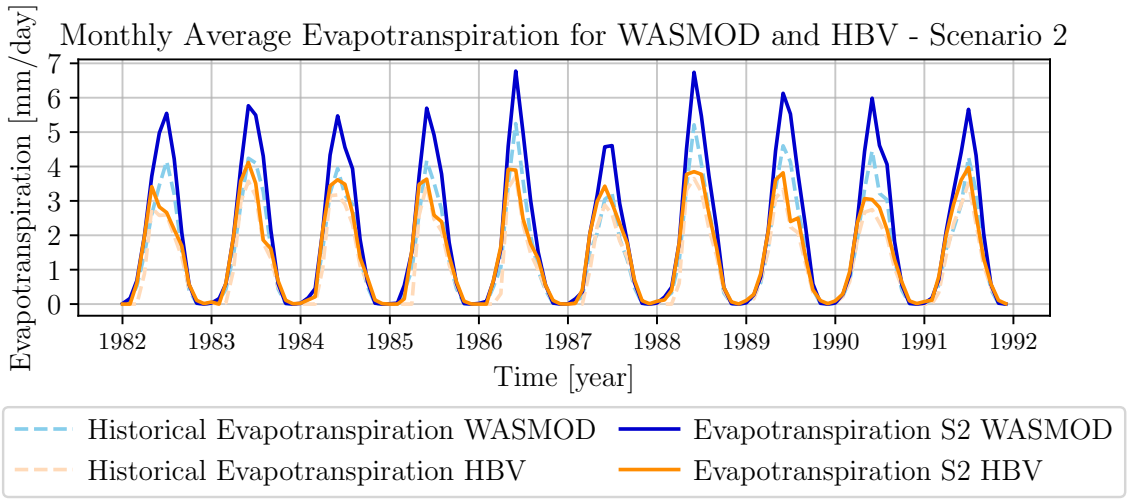

Figure 34: The plot shows the monthly average evapotranspiration for the WASMOD in blue and HBV in orange for the second scenario with an increase in temperature $\Delta T = +3C$ and an increase in precipitation $\Delta P = +15\%$.

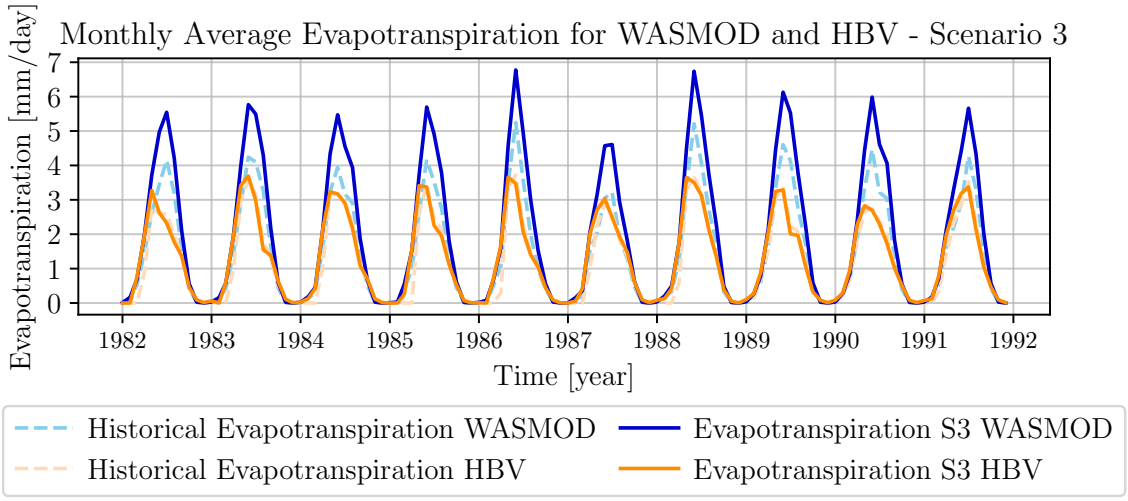

Figure 35: The plot shows the monthly average evapotranspiration for the WASMOD in blue and HBV in orange for the third scenario with an increase in temperature $\Delta T = +3C$ and an decrease in precipitation $\Delta P = -15\%$.

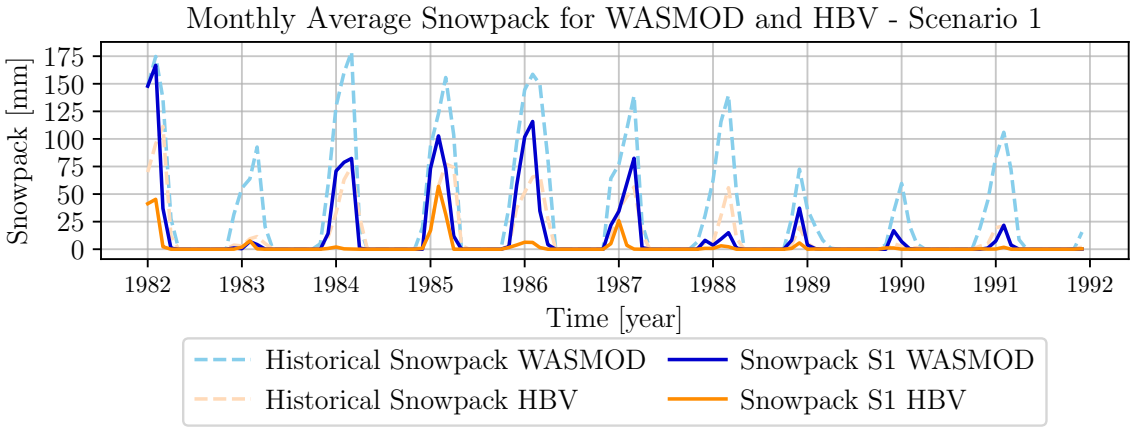

Figure 36: The plot shows the monthly average snowpack for the WASMOD in blue and HBV in orange for the first scenario with an increase in temperature $\Delta T = +3C$ and no change in precipitation $\Delta P = 0\%$.

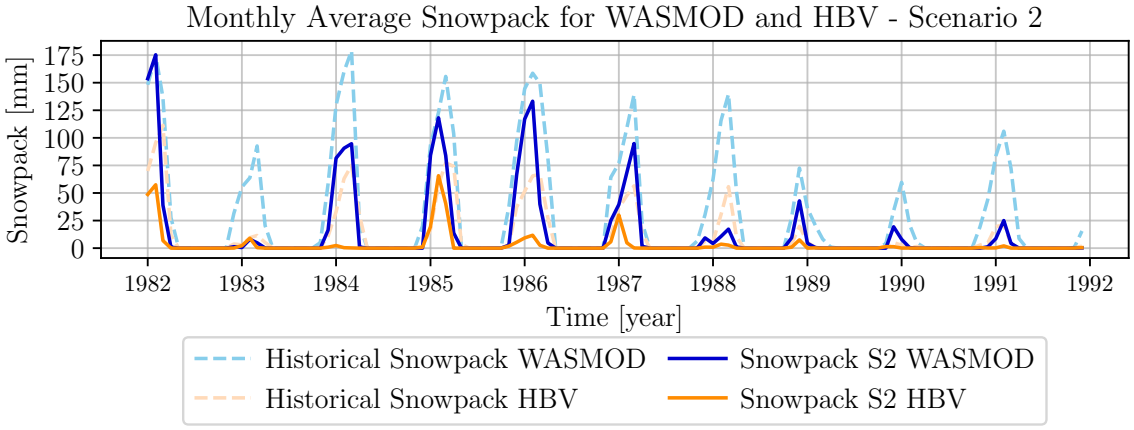

Figure 37: The plot shows the monthly average snowpack for the WASMOD in blue and HBV in orange for the second scenario with an increase in temperature $\Delta T = +3C$ and an increase in precipitation $\Delta P = +15\%$.

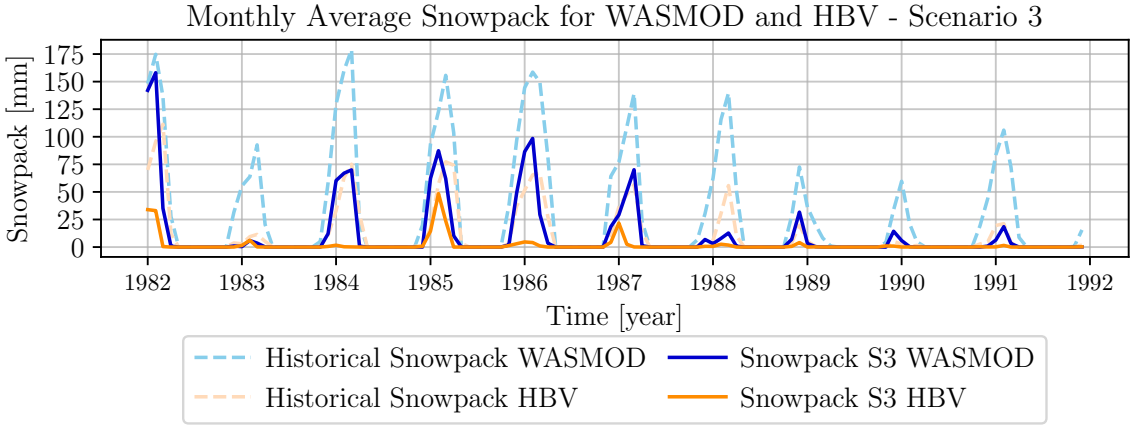

Figure 38: The plot shows the monthly average snowpack for the WASMOD in blue and HBV in orange for the third scenario with an increase in temperature $\Delta T = +3C$ and an decrease in precipitation $\Delta P = -15\%$.

5 Discussion

5.1 Discharge

The observed leftward shift in peak discharge across all scenarios, particularly pronounced in Scenario 3, suggests an alteration in the hydrological cycle, likely due to earlier snowmelt or changes in precipitation patterns. This shift in peak flows could significantly impact the timing and management of water resources, particularly in agricultural and ecological contexts.

The reduction in peak discharge magnitudes raises concerns about decreased water availability during critical periods. It's essential to consider the implications of these findings for flood management and ecological sustainability, especially in riparian ecosystems that depend on seasonal flow variability.

The differences between the HBV and WASMOD models in peak flow predictions, such as WASMOD's higher peaks and a notable double peak in 1984, highlight the variability in model responses to the same climatic inputs. This variability underscores the importance of considering multiple models in hydrological assessments to encompass a broader range of possible outcomes.

5.2 Evapotranspiration

The increase in evapotranspiration peaks observed in WASMOD across all scenarios may indicate a heightened response to temperature changes. This could lead to increased water loss from the system, affecting soil moisture balance and potentially leading to drier conditions, especially in summer months.

The HBV model's stability in evapotranspiration predictions under changing climatic conditions suggests a different approach to modeling soil-plant-atmosphere interactions. Understanding these model-specific responses is crucial for accurately predicting the impacts of climate change on the water cycle and associated ecological processes.

5.3 snowpack

The considerable reduction in snowpack peaks in both models, especially in WASMOD, points to the potential for significant changes in snowmelt dynamics. This could lead to altered runoff patterns, affecting both the quantity and seasonality of water availability in the catchment.

The near elimination of snowpack in most years according to the HBV model is a striking finding, implying a potential shift towards a snow-free catchment under future climate scenarios. This could have profound implications for regions that rely on snowmelt as a primary water source, necessitating a reevaluation of water resource management strategies.

The differential approach to precipitation phase between the HBV and WASMOD models is evident in their respective snowpack simulations. The HBV model utilizes a single threshold temperature parameter (TT) to delineate between snow and rain. In contrast, WASMOD employs a dual-threshold scheme, allowing for a transitional temperature range where both snow and rain can occur. This more nuanced representation in WASMOD may account for its distinct snowpack patterns, particularly under scenarios with increased temperature. As temperature rises, the frequency and intensity of precipitation falling as rain rather than snow can increase, reducing snowpack accumulation as observed in the scenarios presented. This difference in modeling approaches is reflected in the plots, where WASMOD consistently predicts lower snowpack levels compared to HBV, especially in Scenario 3 with decreased precipitation Figure 38. The WASMOD model's dual-threshold method could potentially offer a more gradual transition in precipitation type, which may be more representative of natural processes under warming conditions, leading to earlier and more pronounced reductions in snowpack

6 Conclusion

This comprehensive study examines the hydrological responses of the Åkesta catchment in central Sweden to various climate change scenarios using the HBV and WASMOD models. The findings reveal significant alterations in discharge patterns, evapotranspiration rates, and snowpack levels, indicating a substantial impact of climate change on the regional hydrological cycle.

The study's results, highlighting a shift in peak discharge timing and a reduction in peak magnitudes, signal potential challenges in water resource allocation, flood control, and ecological conservation. These changes necessitate a proactive approach to water resource management, considering the altered hydrological regime.

The contrasting responses of the HBV and WASMOD models, particularly in evapotranspiration and snowpack predictions, emphasize the complexity of hydrological modeling and the importance of employing multiple models to capture a range of potential outcomes. The significant reduction in snowpack, as projected by both models, could lead to drastic changes in seasonal water availability, with far-reaching implications for water supply security, agricultural planning, and ecosystem health.

The findings of this study offer valuable insights for policymakers, environmental managers, and stakeholders, highlighting the urgent need to develop adaptive strategies in response to the evolving impacts of climate

change on water resources. Further research is recommended to refine these model predictions and extend the analysis to long-term impacts, providing a robust foundation for sustainable water resource planning in a changing climate.

References

[Arsenault et al., 2018] Arsenault, R., Brissette, F., and Martel, J.-L. (2018). The hazards of split-sample validation in hydrological model calibration. *Journal of hydrology*, 566:346–362.

[Her and Seong, 2018] Her, Y. and Seong, C. (2018). Responses of hydrological model equifinality, uncertainty, and performance to multi-objective parameter calibration. *Journal of Hydroinformatics*, 20(4):864–885.

[Khu and Werner, 2003] Khu, S.-T. and Werner, M. G. (2003). Reduction of monte-carlo simulation runs for uncertainty estimation in hydrological modelling. *Hydrology and Earth System Sciences*, 7(5):680–692.

[Seibert, 1996] Seibert, J. (1996). Hbv light. *User's manual, Uppsala University, Institute of Earth Science, Department of Hydrology, Uppsala*.

[Seibert and Bergström, 2021] Seibert, J. and Bergström, S. (2021). A retrospective on hydrological modelling based on half a century with the hbv model. *Hydrology and Earth System Sciences Discussions*, 2021:1–28.

[Shen et al., 2022] Shen, H., Tolson, B. A., and Mai, J. (2022). Time to update the split-sample approach in hydrological model calibration. *Water Resources Research*, 58(3):e2021WR031523.

[Vandewiele et al., 1992] Vandewiele, G., Xu, C.-Y., et al. (1992). Methodology and comparative study of monthly water balance models in belgium, china and burma. *Journal of Hydrology*, 134(1-4):315–347.

[Vandewiele et al., 1993] Vandewiele, G., Xu, C.-Y., and Win, N.-L. (1993). *Methodology for Construction Monthly Water Balance Models on Basin Scale*. Vrije Universiteit.

[Xu et al., 2002] Xu, C. et al. (2002). Wasmod–the water and snow balance modeling system. *Mathematical models of small watershed hydrology and applications*, pages 555–590.

[Xu, 1992] Xu, C.-Y. (1992). *Monthly Water Balance Models in Different Climatic Regions*. Phd thesis, Vrije Universiteit Brussel, Belgium. Hydrologie-22, 219pp.

7 Appendix

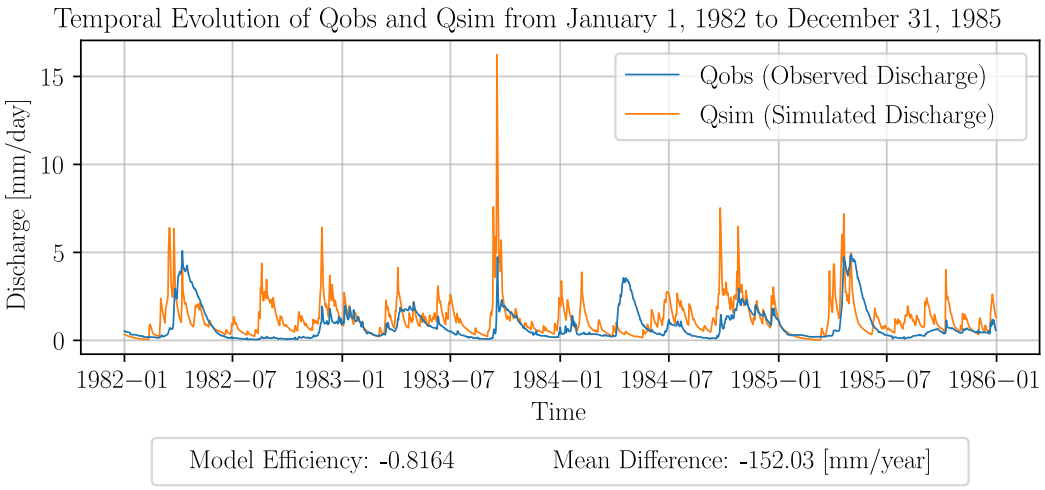

Figure 39: Temporal Evolution of Observed and Simulated Discharge from January 1, 1982, to December 31, 1985. This plot illustrates the daily discharge comparing Qobs (Observed Discharge) in blue with Qsim (Simulated Discharge) in orange. The model efficiency and mean difference for this period are -0.8164 and -152.03 mm/year, respectively, indicating the model's performance against the observed data.

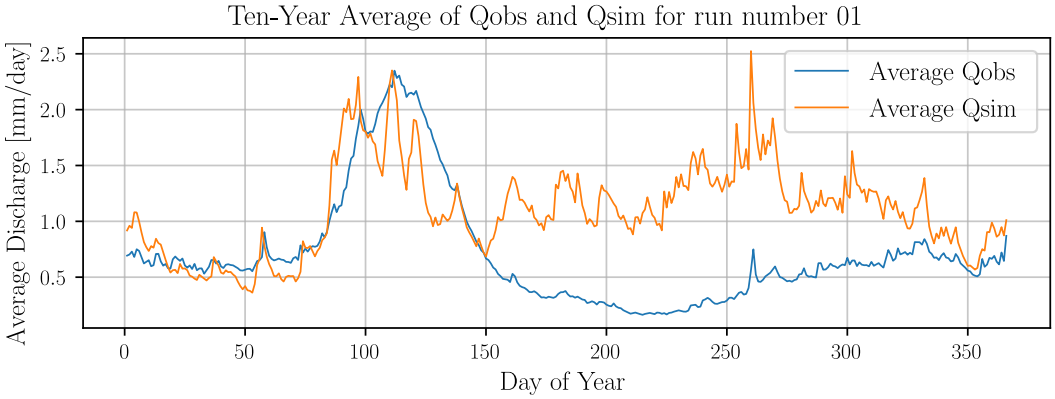

Figure 40: Ten-Year Average of Qobs and Qsim for run number 01. The figure presents the average daily discharge over ten years, showing the comparison between Average Qobs in blue and Average Qsim in orange. The cyclical nature of the discharge is evident, with the simulated values reflecting the observed trends throughout the year.

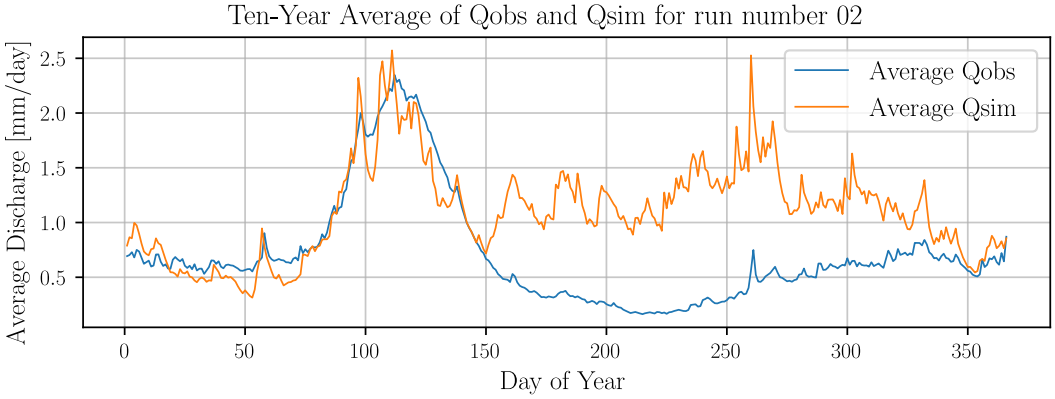

Figure 41: Ten-Year Average of Qobs and Qsim for run number 02. This plot displays the average daily discharge over a decade, comparing Average Qobs (blue) with Average Qsim (orange). The graph highlights the model's ability to capture seasonal variations in discharge, as well as indicating areas where model calibration can be further refined.

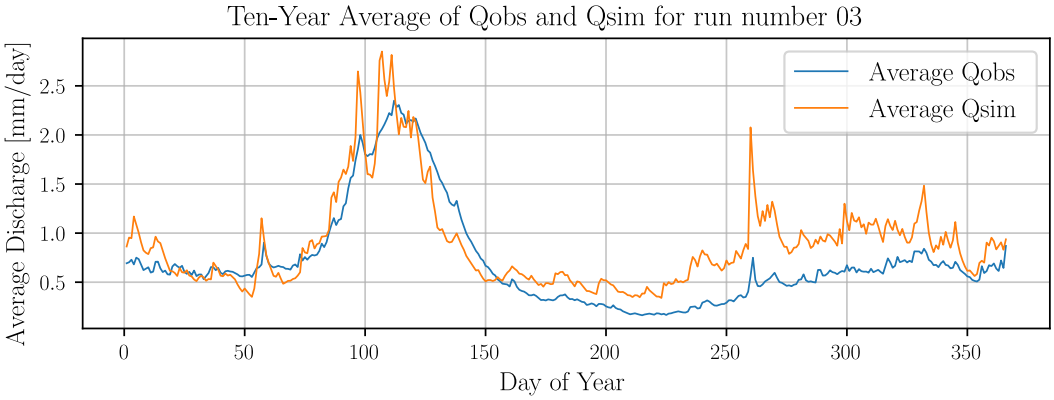

Figure 42: Ten-Year Average of Qobs and Qsim for run number 03. This graph illustrates the averaged observed and simulated discharge over a decade, highlighting the consistency and discrepancies between the model's simulations and the actual measured discharge throughout the year.

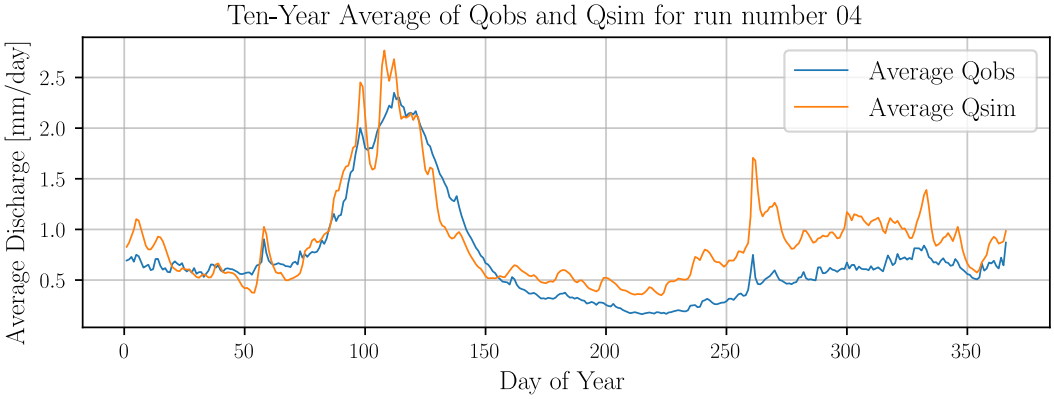

Figure 43: Ten-Year Average of Qobs and Qsim for run number 04. The plot continues to compare the averaged discharge values, providing insight into the model's performance over an extended period, which is crucial for understanding long-term hydrological trends and model reliability.

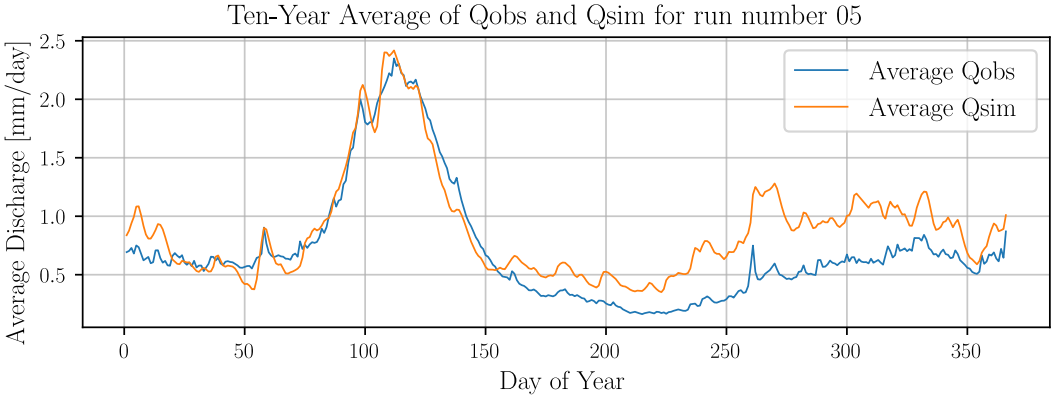

Figure 44: Ten-Year Average of Qobs and Qsim for run number 05. Similar to previous runs, this figure displays the model's ability to simulate discharge against observed data, emphasizing areas of model strength as well as potential periods or conditions where model refinement may be beneficial.

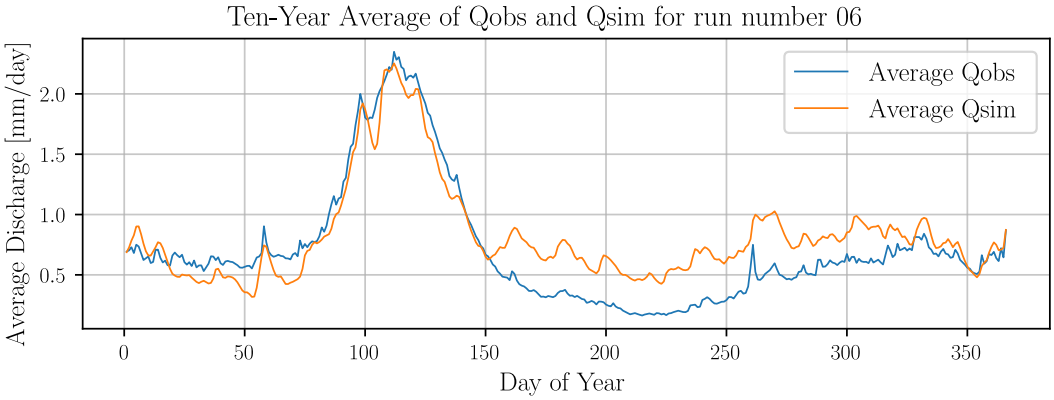

Figure 45: Ten-Year Average of Qobs and Qsim for run number 06. This plot compares the averaged observed discharge with the simulated discharge, allowing for an assessment of the model's performance across different seasons and hydrological events throughout the decade.

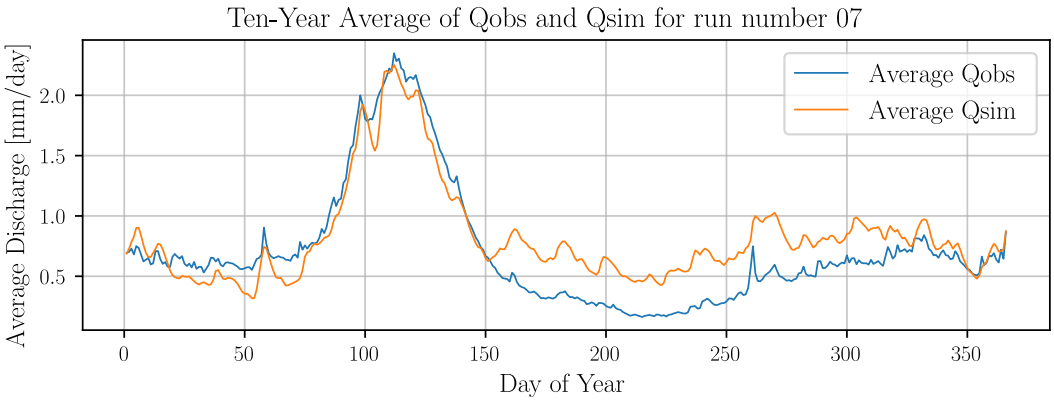

Figure 46: Ten-Year Average of Qobs and Qsim for run number 07. The graph depicts the long-term average discharge patterns, providing valuable insights into the model's capacity to replicate observed hydrological behavior and identify periods of over- or underestimation.

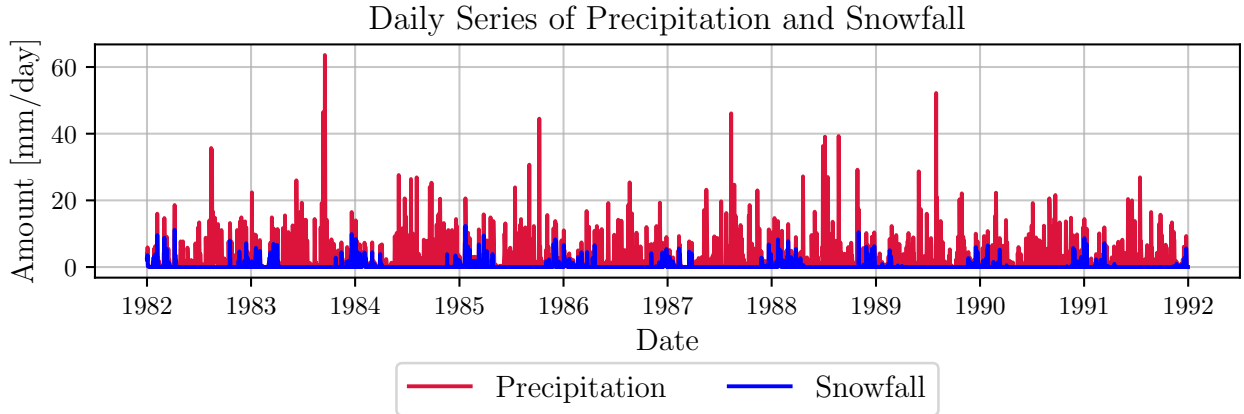

Figure 47: Daily Series of Precipitation and Snowfall. This detailed plot showcases the day-to-day variability in precipitation and snowfall over a ten-year period, highlighting the seasonal distribution and intensity of meteorological inputs that drive the hydrological processes within the model.

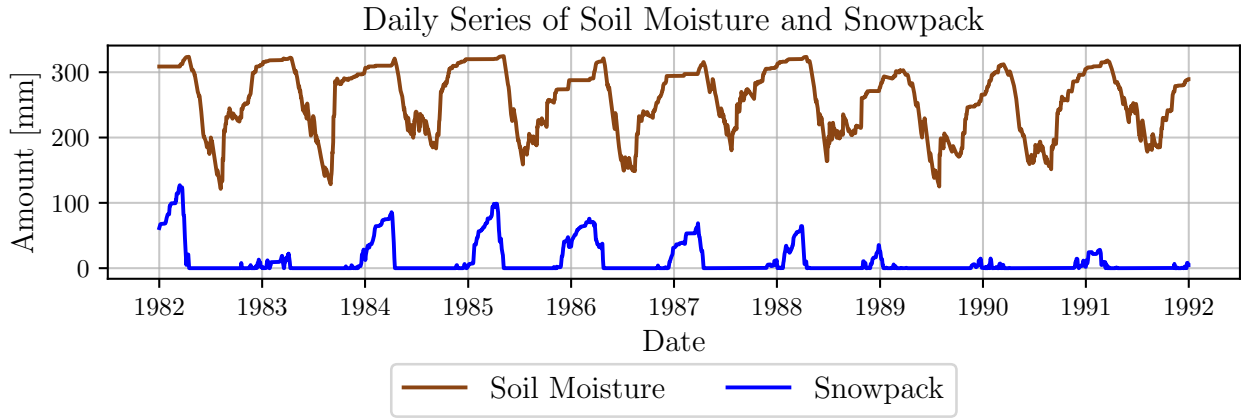

Figure 48: Daily Series of Soil Moisture and Snowpack. This figure displays the day-to-day fluctuations of soil moisture in brown and snowpack in blue over a ten-year period. The contrasting seasonal patterns reflect the hydrological cycle's response to climatic conditions, with soil moisture peaking typically in times of lower snowpack and vice versa, indicating the balance between water retained in the soil and stored as snow.

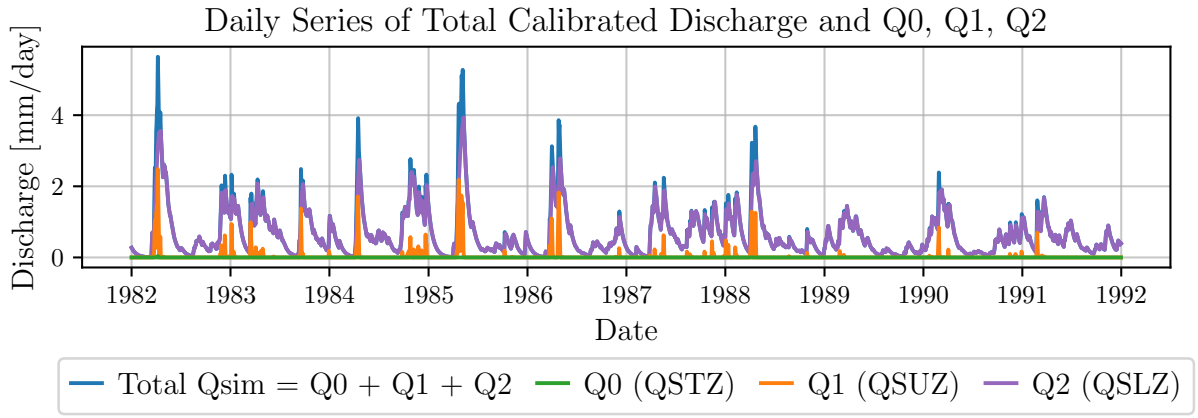

Figure 49: Daily Series of Total Calibrated Discharge and Q0, Q1, Q2. In this plot, the total simulated discharge (Qsim) is shown in blue, with its components: Q0 (quickflow from upper storage, QSTZ) in orange, Q1 (interflow from upper storage, QS1) in green, and Q2 (baseflow from lower storage, QSLZ) in purple. The graph illustrates the relative contributions of each flow component to the total discharge, elucidating the model's ability to capture the complex dynamics of the hydrological processes.

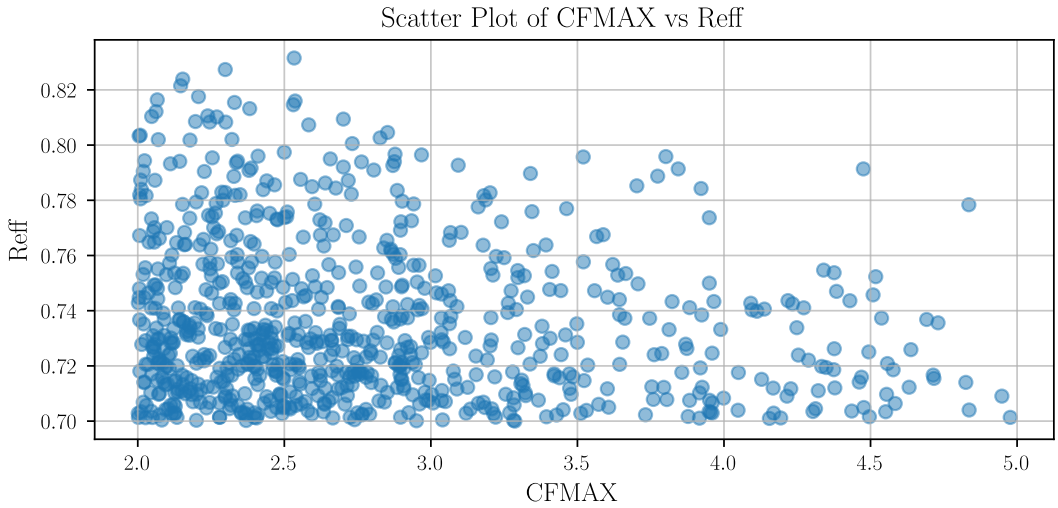

Figure 50: Scatter plot of the parameter CFMAX againt the model efficiency, for $R_{eff} > 0.7$. The plot shows little variation in efficiency when CFMAX is altered in the range (2 to 5.0).

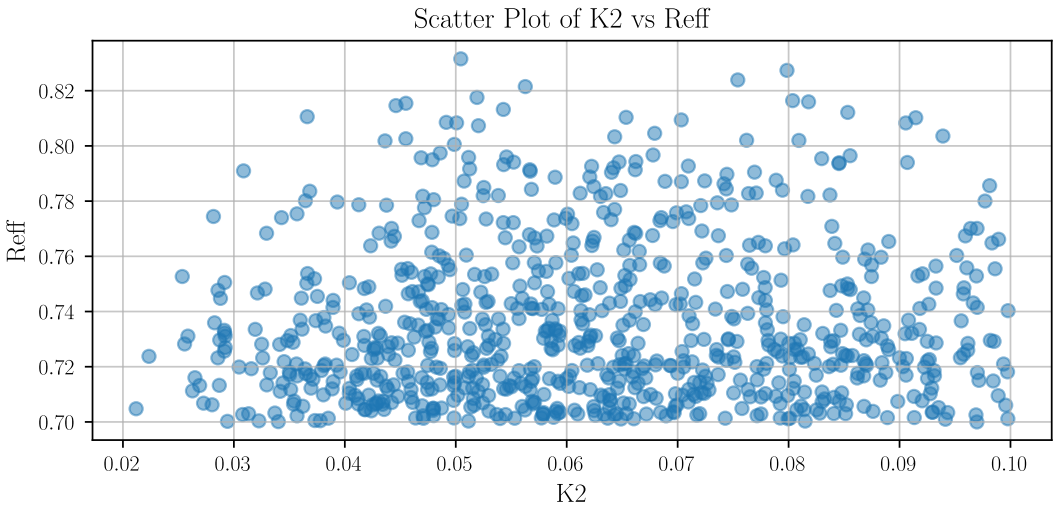

Figure 51: Scatter plot of the parameter K2 againt the model efficiency, for $R_{eff} > 0.7$. The plot shows little variation in efficiency when K2 is altered in the range (0.002 to 0.10).

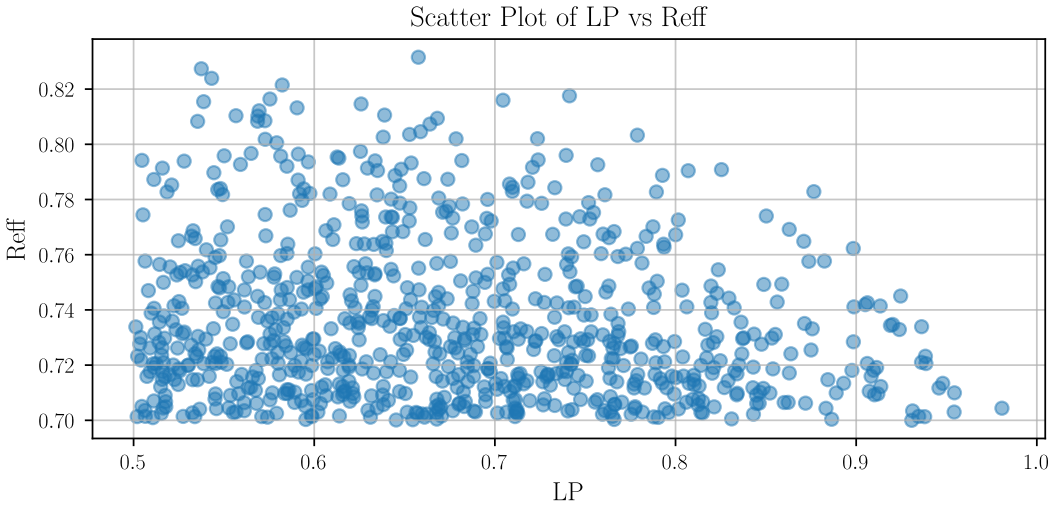

Figure 52: Scatter plot of the parameter LP againt the model efficiency, for $R_{eff} > 0.7$. The plot shows little variation in efficiency when LP is altered in the range (0.5 to 1.0).

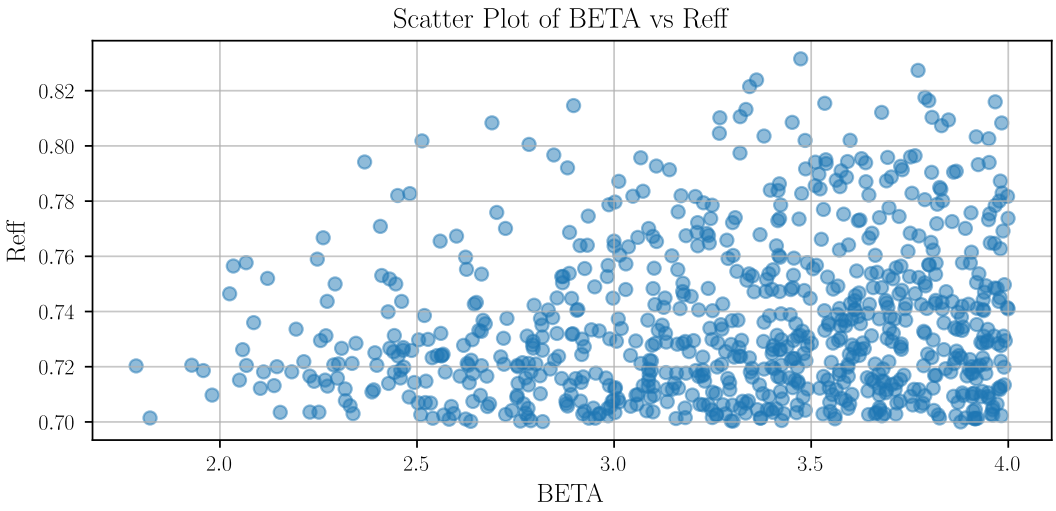

Figure 53: Scatter plot of the parameter MAXBAS againt the model efficiency, for $R_{eff} > 0.7$. The plot shows little variation in efficiency when MAXBAS is altered in the range (1 to 5).

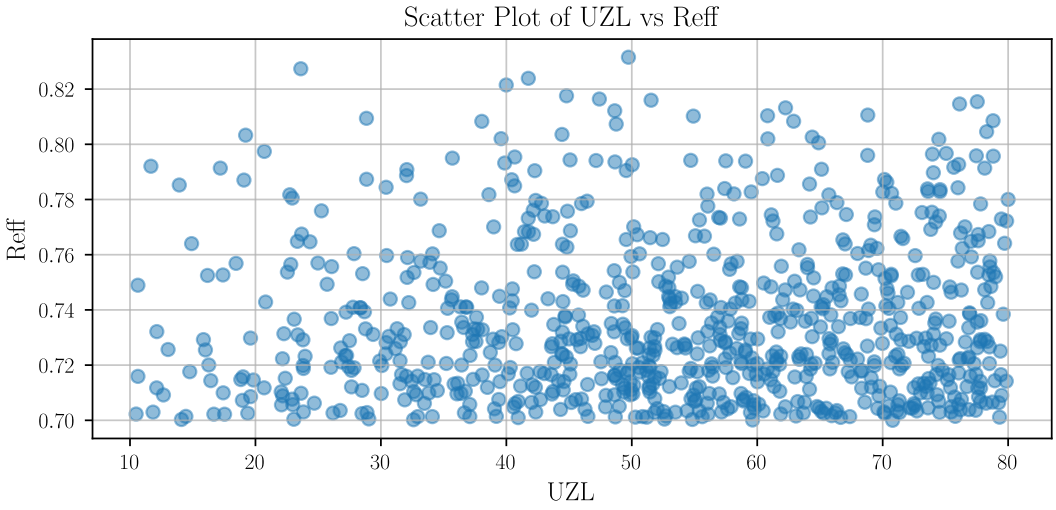

Figure 54: Scatter plot of the parameter UZL againt the model efficiency, for $R_{eff} > 0.7$. The plot shows little variation in efficiency when UZL is altered in the range (10 to 80).